2012-01-01

Investigation On A Gas-Solid Fluidized Bed Hydrodynamics Using A Non-Intrusive Technology To Visualize Flow Field

Md Rashedul Hasan Sarker
University of Texas at El Paso, mhsarker@miners.utep.edu

INVESTIGATION ON A GAS-SOLID FLUIDIZED BED HYDRODYNAMICS USING A NON-INTRUSIVE TECHNOLOGY TO VISUALIZE FLOW FIELD

MD RASHEDUL HASAN SARKER

Department of Mechanical Engineering

APPROVED:

Norman Love Jr., Ph.D., Chair

Ahsan R. Choudhuri, Ph.D.,

Chunqiang Li, Ph.D.

Benjamin C. Flores, Ph.D.
Interim Dean of the Graduate School

Dedication

To my parents

INVESTIGATION ON A GAS-SOLID FLUIDIZED BED HYDRODYNAMICS USING A NON-INTRUSIVE TECHNOLOGY TO VISUALIZE FLOW FIELD

by

MD RASHEDUL HASAN SARKER, B.S.ME

THESIS

Presented to the Faculty of the Graduate School of

The University of Texas at El Paso

in Partial Fulfillment

of the Requirements

for the Degree of

MASTER OF SCIENCE

Department of Mechanical Engineering

THE UNIVERSITY OF TEXAS AT EL PASO

August 2012

Acknowledgements

I would like to thank my parents for my education I was fortunate to have. I would also thank to my brothers, sisters and friends to support during my graduate degree at UTEP. It's a great honor for me to work with supervision of my advisor Dr. Norman Love. His expert guidance helped me to become a better engineering student.

I would also like to thank members of my thesis committee Dr. Ahsan Choudhuri and Dr. Chunqiang Li for their insight comments, revision and participation in my thesis presentation. Also it's a pleasure to thank all of my colleagues in Center for Space Exploration Technology Research (cSETR) lab for their contribution during my research work. Finally, I would like to thank Olympia Caudillo, M.Ed. for her time and consideration for reviewing and formatting my thesis.

Abstract

The biggest challenge for 21st century is to fulfill global energy demand and at the same time reduce detrimental impact on environment. Gasification technology can meet the requirement and also reduce emission without compromising its performance. In coal gasification, instead of burning coal completely a partial combustion takes place with presence of steam and limited amount of oxygen. In this controlled environment a chemical reaction takes place and produces a mixture of clean synthetic gas. Gas-solid fluidized bed is one type of gasification technology. During gasification mixing behavior of solid (coal) and gas and their flow pattern very complicated to understand. Many attempts have taken in laboratory scale to understand bed hydrodynamics with spherical particle whereas in actual coal are non-spherical. Considering this issue an attempt has taken to investigate fluidized bed behavior using different ranges non-spherical particles and spherical particle as well. Different parameters are controlled during investigation like particle size, bed height, bed diameter and particle shape. Particles used from 355 μm to 1180 μm, bed diameter varied from 2 cm to 7 cm, two fluidized bed with diameter 3.4 cm and 12.4 cm, spherical and non-spherical shape particles were taken into consideration for investigation. Pressure drop was measured with increasing superficial gas velocity. The velocity required to start fluidize the particle is called minimum fluidization velocity. Minimum fluidization velocity is one of the most important parameter to design and optimize gas-solid fluidized bed performance. This minimum fluidization velocity was monitored during investigation with changing factors that affect this velocity. From investigation it has been found that minimum fluidization velocity is independent on bed height for both spherical and non-spherical particles, it decrease with decreasing particle size and it also decrease with decreasing bed diameter. Shadow sizing a non-intrusive technology is also used to visualize flow field inside fluidized bed in dilute section for both spherical and non-spherical particles and also detect the particle size.

Table of Contents

List of Tables

List of Figures

Chapter 1: Introduction

1.1 OVERVIEW

For a long period of time liquid and gaseous fuels played an important role on worldwide industrial and technological development. Research and development is also going on alternative energy source like coal and other solid fuels combustion (1). Where our modern life is fully depending on energy, it is mandatory to produce clean and climate friendly energy technology. Combustion of coal generally exposes its constituents like sulfur, nitrogen, carbon to oxidation process and unwanted pollutant emissions. Producing necessary energy and at the same time reduce unwanted pollutant emissions is the biggest challenge for 21st century. Coal gasification is such a technology that can produce energy and reduce some emissions without sacrificing its performance. Fluidized bed technology is one method to convert coal or other feedstock into synthetic gas (CO-H2). This method breaks the solid fuel into their molecular level and removes the impurities and ash. The U.S. Department of Energy is emphasizing on coal gasification with enhance reliability and efficiency (2). Significant development in coal burning technology such as fluidized bed has been observed in last quarter century. Most of cases popular choice of fluidization particularly with coal particles is gas-solid fluidization. Flow pattern and solid mixing in fluidized bed are the important design parameter. Moreover multiple scales with interaction gas-solid phase fluidized bed are difficult to access (3). To characterize fluidized bed minimum fluidization velocity is the most important parameter. Many factors that influenced minimum fluidization velocity described in literature review chapter.

Experimental data is required to get detail information of gas-solid fluidized bed behavior. To understand gas-solid fluidized bed behavior a laboratory scale fluidized bed designed and constructed with available materials in market. Borosilicate glass beads were used as test particles and supply of air to test particles as gasifying agent. Different particle size ranges and different shapes were used to

observe effect of particle size and shape. Pressure drop with increasing superficial gas velocity was measured to investigate fluidized bed behavior.

High speed imaging and shadow sizing technology was also used to observe flow field inside fluidized bed. Shadow sizing technology is a non-intrusive method to visualize flow field and it can also detect the particle size, particles velocity over size.

1.1 RESEARCH OBJECTIVES

The purpose of this study is to investigate fluidized bed behavior with changing different parameter. Minimum fluidization velocity is one of the main design factors of fluidized bed that affected by changing different parameter in fluidized bed. Particle size, shape, bed height, bed diameter are the parameters on what minimum fluidization depends. This thesis outlines with the following objectives.

1) Hydrodynamic behavior of fluidized bed with spherical and non-spherical particles.
2) Flow field visualization for spherical and non-spherical particles using a non-intrusive technology.

1.2 THESIS ORGANIZATION

Chapter 1 summaries the importance of coal gasification and one coal gasification method fluidized bed. Research objectives and available facilities also describes in this chapter. Chapter 2 summaries literature review regarding available gasification technology, their uses, and different type's fluidized bed, different types of particles density, particles size, shapes and bed diameter. Chapter 3 describes about experimental setup, their design parameter, particles selection and production method, test matrix, experimental measurement methods and technical consideration to compare between theoretical findings and experimental results. Chapters 4 describe experimental results, discussion about

findings and compare them with theoretical explanation. Finally, chapter 5 summaries the experimental finding with conclusion about our research and recommended future works.

1.4 FACILITIES

All the analysis and experimental testing were performed in Center for Space Exploration Technology Research (cSETR) laboratory in Mechanical Engineering Department at The University of Texas at El Paso (UTEP). The lab is fully equipped with wide range of instruments with 5 HP blower, hydraulic compressor, high speed camera, sieve shaker, microscopic camera, flow meter, differential manometer etc. to perform experimental measurement.

Chapter 2: Literature Review

2.1 GASIFICATION

Gasification is a technology that converts carbonaceous materials into synthetic gas. Low value feedstock (carbonaceous materials) turns into a high value product (synthetic gas). In a chemical reactor the carbonaceous materials placed with limited amount of steam and oxygen. With this controlled environment a chemical reaction takes place that produce a mixture of gas containing carbon monoxide (CO), hydrogen (H_2) and other gaseous compounds. This mixture of gas termed as "Synthetic Gas". Gasification process breaks the feedstock into their molecular level by which it removes impurities and high temperature drives out ash from feedstock which ensures a clean production of synthetic gas. Gasification is really a breakthrough technology. Although synthetic gas has lower heating value then natural gas it still be used for high-efficient combined cycle electric power plant or to make many products presently made from natural gas such as ammonia fertilizer, methanol derived chemicals. (4)

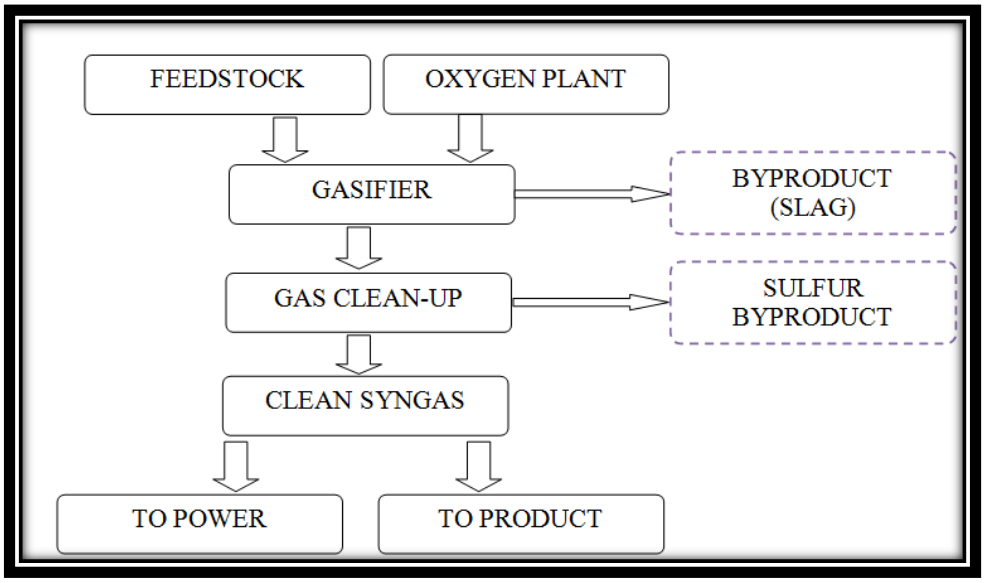

Figure 2.1: The Gasification Process

Figure 2.1 shows the steps of gasification process. For a gasifier a wide range of feedstock can be used like coal, oil refineries liquid residuals and waste of chemical plants and biomass. Gaseous and liquid feedstock feed into gasifier directly and on the other hand solid feedstock breaks down into very small particles and then feed into gasifier. Glass like byproduct slag produced from solid and liquid feed gasifier which is no-hazardous. Slag can be used in road construction and for roofing materials. From most gasification plants 99% sulfur removed and recovered as elemental sulfur or sulfuric acid. Before using raw synthetic gas impurities should be removed. Sulfur, mercury, uncovered carbon, trace minerals, particulates are removed by processes common to the chemical and refining industries. Finally clean syngas is combusted into high-efficient combined cycle electric power plant and to make products like substitute natural gas, chemicals, fertilizers, transportation fuels and hydrogen. (5)

2.1.1 Combustion Vs Gasification

Combustion is a complete oxidation process to produce thermal energy. The hazardous byproducts produce for complete combustion or burning of coal. Solid wastes, NOx, SO_2, and CO_2 have the most detrimental impact on our environment. Furthermore, burning coal is dirty, controlling and capturing of CO_2 is difficult.

On the other hand gasification is called partial oxidation. Gasification process burns the carbonaceous materials partially instead of burning it completely. This process converts carbonaceous materials into synthetic gas which can be used to produce electricity and high value products like fertilizers, chemicals, hydrogen and transportation fuels. Furthermore, it produces non-hazardous by products and nearly zero emissions. (6)

2.1.2 Chemistry in Gasification

The carbonaceous materials go through different processes during gasification in a gasifier. The chemical reaction takes place with presence of steam and limited amount of oxygen. When feedstock feeds into gasifier dehydration process occurs at temperature reaches up to 100^0 C. At this point the moisture contents from feedstock drives out in the form of gas. When temperature goes up to 200-300^0C pyrolysis or devolatilization process occurs. As temperature increases the feedstock goes through decomposition process and release volatiles contents in the form of gas. At this point feedstock (for coal) losses its weight up to 70% due to release of volatile contents and the remaining is called char. Volatile contents are tars, H_2, CH_4. (7)

The released gas form has higher sulfur, hydrogen and oxygen contents than feedstock. On the other hand remaining char is mixture of carbon-rich organics.

Released volatile contents and remaining char react with oxygen to produce carbon dioxide (CO_2) and heat. This continuous generation of heat energy is required for pyrolysis and gasification reactions further. (7)

The basic reactions are

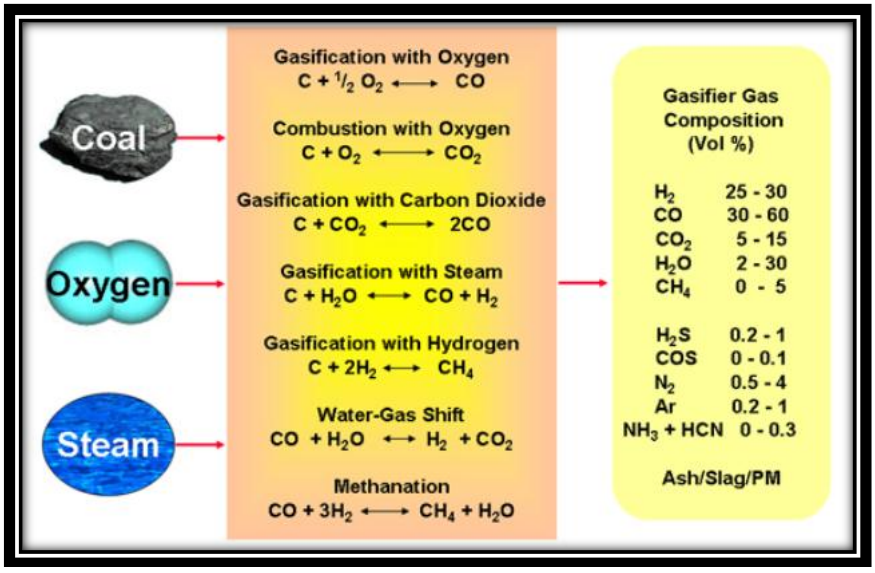

Figure 2.2: Gasification Reactions (8)

2.1.3 History of Gasification

In early-1800s gasification technology was invented but in last 50 years it has gone rapid transformation. Rapid changes of gasification can be categorized into following five stages. (4)

1850-1940: Before the development of natural gas all gas for fuel and light were produced by gasification of coal. This gas was called 'Town Gas'.

1940-1975: During World War II gasification technology was used to produce synthetic gas by German Engineers. Later this technology was exported to South Africa (1950) where it was developed further to produce chemicals and liquid fuels.

1975-1990: For pursuing energy crisis the U.S. government started financial support for several proof-of concept gasification projects like Integrated Gasification Combined Cycle (IGCC) electric power plant.

1990-2000: At this stage government agencies of United States and Europe started providing financial support for four medium sized (≈ 250MWe) projects to demonstrate the feasibility of IGCC process.

2000-present: New IGCC power plants started by commercial developers without government subsidies. These new facilities are adjacent to refineries where hydrocarbons and petroleum coke are available.

2.2 GASIFICATION TECHNOLOGY

Depending on flow of gasifying agents gasification technology categories into three sections.

2.2.1 Fixed or Moving Bed

Figure 2.3 shows a diagram of generic moving bed. In moving bed feedstock and gasifying agent interact with counter flow. Feedstock feeds from top of the bed and steam, oxygen introduce from

bottom of the bed. Before using feedstock they are made into coarse particles for better permeability and to avoid excess pressure drop and chemical burning. As the feedstock falls down it goes different gasification stage, leaving only syngas and a dry or molten ash. Ash goes out from the bottom of bed. Movieng bed runs in dry-ash mode and in slugging mode. In dry-ash mode temperature is controlled under ash slagging tempureature with excess steam. Excess steam cooled the ash and make solid ash. On the other hand in slagging mode less steam is provided to get higher temperature. This high temperature melts the ash and produce solid slag (9)

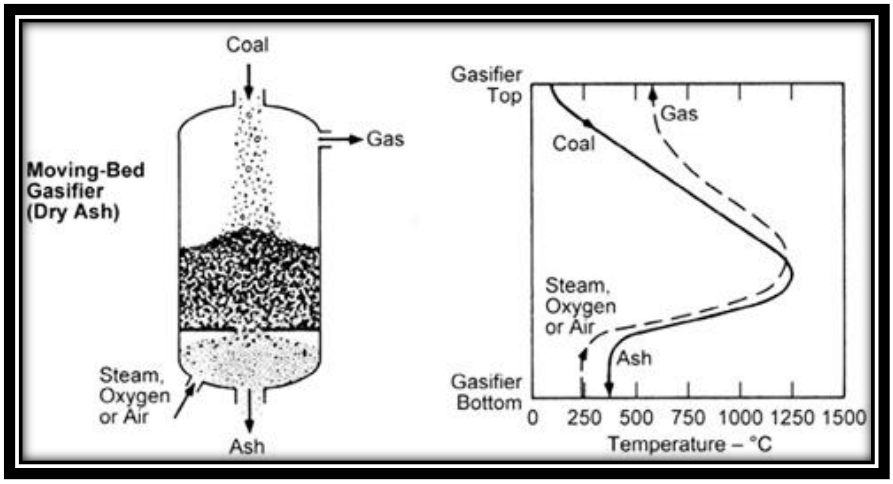

Figure 2.3: Moving Bed Gasifier (9)

2.2.2 Entrained Bed

At this type of bed feedstock and gasifying agent feed together from top of bed. Feedstock and gasifying agent goes into same direction and gasifying agent surround the coal particles as they flow and passes different stages of gasification. This type of bed operated at high temperature to melt the ash into slag. Furthermore entrained bed can use dry or wet feedstock. Practically they can handle any coal feedstock and can produce tar free, clean syngas (10).

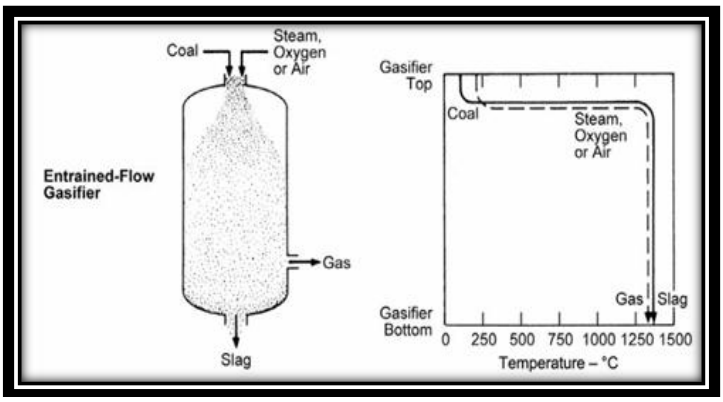

Figure 2.4: Entrained Flow Gasifier (10)

2.2.3 Fluidized Bed

In this type of bed high velocity of upward flow of gasifying agent introduced to the feedstock. Upward flow makes the feedstock suspended and various stages of gasification takes place. This type of bed provides back mixing and mixes the new feed coal with undergoing gasification coal. Less than 6 mm particle size used to maintain suspension of particles into the bed. It operates at significant high temperature for acceptable carbon conversion rate but less than ash fusion temperature to avoid clinker and de-fluidization of bed. This type of gasifier is suitable for coal and other type of fuel like biomass (11).

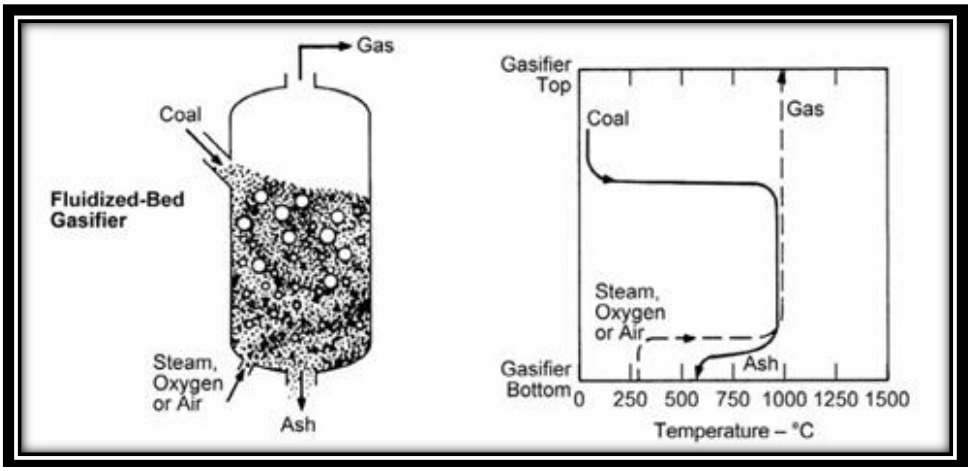

Figure 2.5: Fluidized Bed (11)

2.3 MULTIPHASE FLOW

Generally a phase is identified by solid, liquid or gaseous state. A flow is referred to a multiphase flow when the flow contains mixture of two or more than two phase with different volume fraction.

Disperse flows and Separated flows are two identified topologies of multiphase flow. Dispersed flow contains discrete elements distributed as a connected volume in a continuous phase like bubbles in liquid and droplets in gas. Separated flows contain two or more phases of different fluid separated by a line of contact. (12)

2.3.1 Types of Multiphase Flow

Most widely used multiphase flows are two-phase flows. Gas-liquid flows, liquid-solid flow, gas-solid flows.

Gas-liquid flows contain gas bubbles in liquid flow or liquid droplets in gaseous flow. Process industries are interested to use this type of flow. Formation of droplets of combustible liquid fuel is very important for internal combustion engine, spray formation with droplets for processing materials. Also in heat exchanger the use of steam water flow are very common.

Liquid-solid flows contain solid particles in liquid phase. It is also called slurry flows. This type of flow is mainly used for transportation of solid particles.

Gas-solid Flows contain suspended solid particle by gas. Gasification is a perfect example of gas-solid flows. In fossil fuel power plant, the combustion of coal depends of coal particle burning and suspension of coal particles into gasifying agents. Cyclone separator and electrostatic precipitators are also use the principle of gas-solid flow. Moreover, gas-solid flows are also used for pneumatic transportation. (12)

2.4 FLUIDIZED BED REACTORS

In modern society most of our energy comes from the source of carbonaceous fuel. This carbonaceous fuel can be found in solid form or in liquid form which required more processing than natural gas considering environmental impact. Fluidized bed reactors are simple chemical reactor for

combustion, heat transfer process, steam generation, power plant and chemical synthesis. Moreover, this technology is really a breakthrough technology that can reduce significant amount of emission after partially burning carbonaceous fuels. Coal and biomass are the major source of carbonaceous fuels. Because of effectiveness of this technology concerning about environmental issue currently a great industrial interest has been found. (13)

Based on flow behavior of carbonaceous particles and gasifying agent fluidized bed reactor can be classified by following types. (14)

Stationary or Bubbling Fluidized Bed runs with low gas velocity that practically tries to balance the weight of particles. At this point particles suspended on the gasifying agent as their weight is balanced by low gas velocity. Also the particles behave like boiling liquid depending on particles characteristics like size and density. Particles remain on the surface except some fine particles that entrained.

Vibratory fluidized Bed is like stationary fluidized bed including external source of vibration introduced to bed for better excitement and improving mixing property of particles with gasifying agent.

Circulating Fluidized Bed runs relatively with high velocities that expand the solid particles beyond their suspension. High velocity entrained the particles from bed and which is separated from gas by cyclone separator and re-enter to bed witch closed loop. Moreover, an internal circulation also takes place for those particles which are not entrained out from the bed with high velocity.

Transport or Flash Reactor Bed has higher gas velocity than the circulating fluidized bed. Velocity difference of gas and particle decreased more than the circulating fluidized bed. Particle velocity reaches near the velocity of gas. Only some selected application used this reactor where solid retention times are significantly sufficient.

In **Annular Fluidized Bed** a central nozzle is introduced at the middle of bed with additional gasifying agent. A good intense mixing zone achieved above the nozzle compare to external loop of circulating fluidized bed. Moreover, annular fluidized bed can be connected with other fluidized bed.

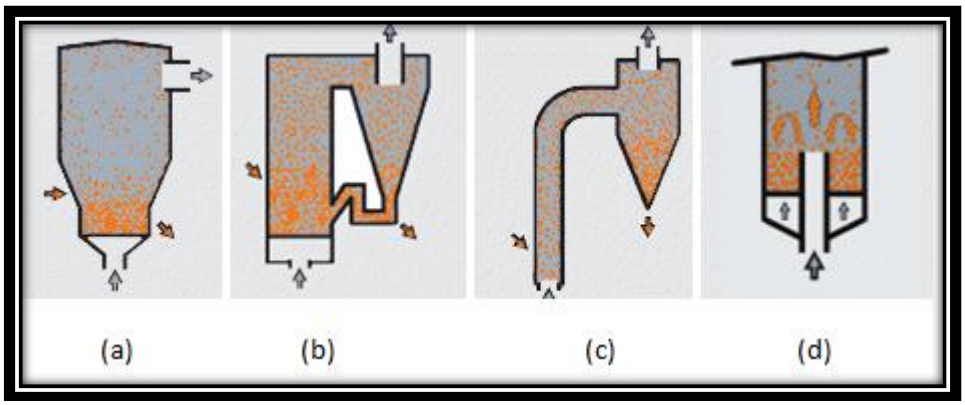

Figure 2.6: (a) Bubbling Bed (b) Circulating Bed (c) Transport Bed (d) Annular Bed (14)

2.4.1 Gas-Solid Fluidization

Gas-solid fluidization follows a simple principle. Upward flow of gasifying agent (steam/air) introduced into a packed solid bed. As a result a pressure drop occurs within the bed. This pressure drop goes as high as equal to weight of the solid particles. Characteristics of fluidization depend on different factors. Properties of solid particle are the important factor on which behavior of fluidization depends. Fluidization behavior also depends on solid particle size, particle density, their cohesiveness etc. In 1973 Geldart suggested four classified types of particles range as follows (based on density and size) depending on what fluidization behavior can be categorized. (15)

Group A composed with small particle size with low density less than 1400 kg/m^3. Bubbles appear after the minimum fluidization velocity and also the bed expand after minimum fluidization velocity. A smooth fluidization occurs with low velocity. Cracking catalyst powder is in group A.

Group B composed with particle size range between 40 μm to 500 μm and density between 1400 kg/m^3 to 4000 kg/m^3. Bubbling appears at minimum fluidization velocity and these bubbles do not depend on particle size. Sand like powder is in group B.

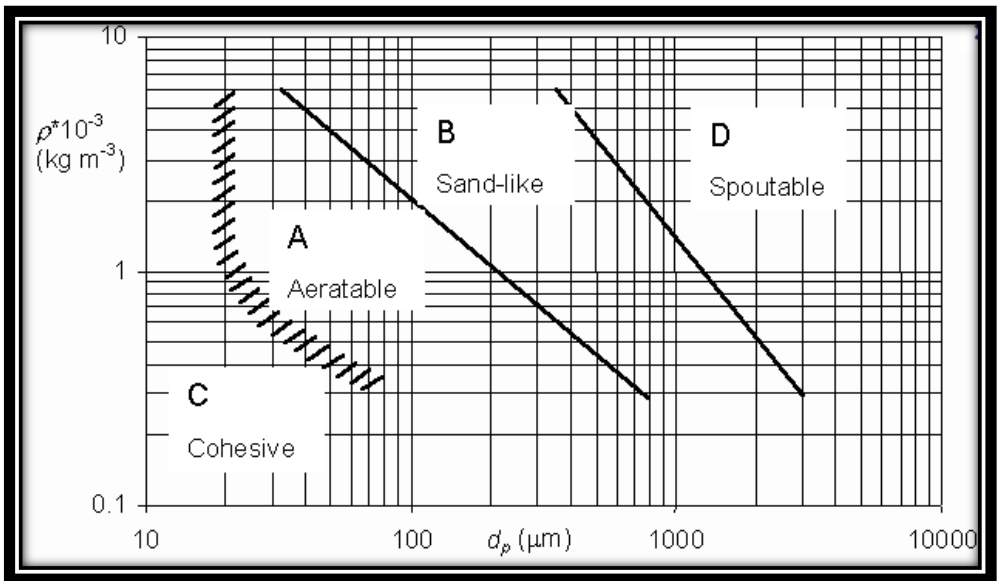

Figure 2.7: Geldart's Classification of Powder according to fluidization properties.

Group C composed with all cohesive powder. Particles of this group are extremely fine and very much difficult to fluidize because there highly cohesive property. To fluidize the group C particles it is recommended to use stirrers or vibration to break the inter-particle forces. Flour, cement are example of this group.

Group D composed with relatively large or dense particles and easily spout. During fluidization large bubble or channeling occurs for this group of particles.

2.4.2 Fluidization Regimes

There are at least five fluidization states that have found in gas-solid flow. The transition of these different fluidization regimes depends on gas-solid system properties. All fluidization regimes can be categories into two sections – particulate (smooth) and aggregative (bubbling).

Before particulate fluidization the particles are fixed until minimum fluidization. The superficial gas velocity (u) is less than minimum fluidization velocity ($0 \leq u < u_{mf}$ (minimum fluidization velocity). This state is referred as fixed bed.

When superficial gas velocity reaches up to minimum fluidization velocity (u_{mf}) the fixed bed begins expand smoothly with low pressure fluctuation. At this point small-scale of particles motion and

tendency to aggregate observed. This state is referred as particulate fluidization where $u_{mf} \leq u < u_{mb}$ (superficial velocity at onset of bubbling). It is also called homogeneous fluidization.

From the point of onset bubbling fluidization bubble appears near at distributor. These bubbles coalescence and rise to top of the bed surface. The top surface is well identified as the bubbles break at top surface. In bubbling fluidization pressure fluctuation is irregular and at this point superficial gas velocity is between $u_{mb} \leq u < u_{ms}$ (slugging velocity)

For increase of superficial gas velocity after bubbling fluidization the bubbles mostly fill the bed column and rises the top surface with collapse of large bubbles. This state is referred as slugging fluidization and gas velocity is between $u_{ms} \leq u < u_k$ (velocity at transition to turbulent regimes).

At turbulent regimes the particles cluster moves to and fro with low amplitude pressure fluctuation and top surface can barely identified. At this point the gas velocity is between $u_k \leq u < u_{tr}$ (vertical transport velocity)

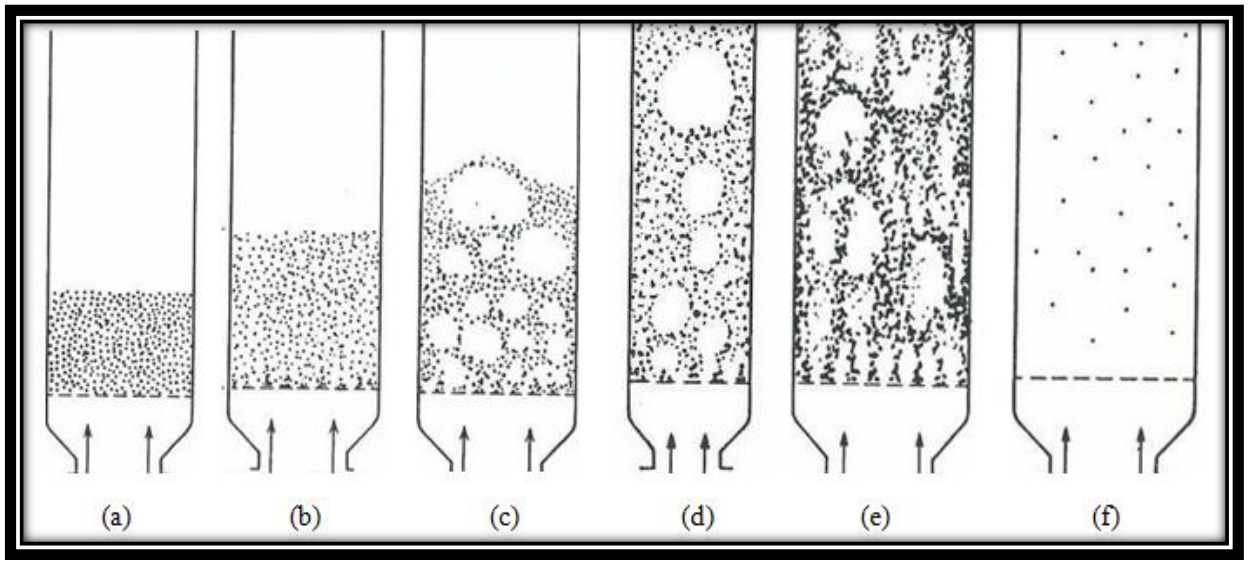

Figure 2.8: (a) Fixed Bed (b) Particulate Fluidization (c) Bubbling Fluidization (d) Slugging Fluidization (e) Turbulent Fluidization (f) Fast Fluidization

In fast fluidization particles transport from top of the bed column and there is no upper bed surface. The bed getting empty for transport of particles and should add more particles by near bottom of the bed.

All the above fluidization regimes do not happened for any particular fluidized bed because transition point depends on different features. Minimum fluidization and bubbling velocity depends on gas-solid properties. Slugging velocity depends on bed height and bed column diameter and turbulent velocity depends on feeding rate of particles to the bed. (16)

2.5 GAS-SOLID FLUIDIZED BED REACTORS

Petroleum industries have extensive use of fluidization and also for gas-solid reactions, catalytic processes, and acrylonitrile synthesis. Pressure drops, minimum fluidization velocity are the most important parameter to characterize the gas-solid fluidized bed.

2.5.1 Pressure Drop

Typically a fluidized bed filled with small solid particles. Flow of gasifying agent passes through the packed bed and the gas flow experienced a resistance. This resistance is the resultant of drag force exerted by the solid particles in bed. For passing the flow at a specified flow rate through bed for proper mixing both gas and solid phase a pressure drop is required. This pressure drop through bed is commonly measured from the total drag force exerted by the solid particles. (17)

To measure the bed pressure drop Sabri Ergun in 1952 expressed bed frictional factor as a function of Reynolds number. (18)

$$f_p = \frac{150}{R_e} + 1.75 \quad (1)$$

Where,

$$f_p = \left(\frac{\Delta P}{L}\right)\left(\frac{Dp}{\rho V_s^{\,2}}\right)\left(\frac{\varepsilon^3}{1-\varepsilon}\right) \quad (2)$$

$$R_e = \frac{D_p\, V_s \rho}{(1-\epsilon)\mu} \quad (3)$$

Here,

$\Delta P = Pressure\ Drop$

$L = Length\ of\ the\ Bed$

$D_p = Diameter\ for\ spherical\ particles$

$\rho = Fluid\ density$

$\mu = Dynamic\ Viscosity\ of\ Fluid$

$\varepsilon = Void\ Fraction$

$V_S = Superfical\ Gas\ Velocity$

Putting the value of frictional factor and Reynolds number from equation (2) and (3) in equation (1), the bed pressure drop comes as follows,

$$\Delta P = \frac{150(1-\varepsilon)^2 \mu}{D_p{}^2 \varepsilon^3} L V_S + \frac{1.75 \rho_f (1-\varepsilon)}{D_p \varepsilon^3} L V_s{}^2 \quad (4)$$

Changing in pressure drop in equation (4) is subjected to solid particles equivalent diameter (D_P) and void fraction of the bed (ϵ).

On the other hand, Ergun equation (equation 4) is not straight forward for non-spherical particles. In equation 4, D_p is the diameter of spherical particles which is straight forward. But for non-spherical particles, their equivalent diameter was used where,$D_{eq} = \varphi \times D_{sd}$. Here D_{sd} is the Sauter-mean diameter (19). For non-spherical particles the bed pressure drop equation will be,

$$\Delta P = \frac{150(1-\varepsilon)^2 \mu}{D_{eq}{}^2 \varepsilon^3} L V_S + \frac{1.75 \rho (1-\varepsilon)}{D_{eq} \varepsilon^3} L V_s{}^2 \quad (5)$$

2.5.2 Minimum Fluidization Velocity

At the onset of fluidization or minimum fluidization velocity the upward force by flow is equal to the gravitational force exerted by bed particles. In other way, pressure drop across bed is equal to total weight of bed particle per unit area of cross section. (17)

Minimum fluidization velocity can be calculated by balancing net weight of bed particle by upward flow force of gasifying agent.

Upward force = $\Delta P \times A$

For a fixed bed height (L) with void fraction (ϵ), volume of particles = $(1-\epsilon)A \times L$

Net weight of particles = $(1-\epsilon) \times (\rho_p - \rho_f) A \times L \times g$

Here,

ρ_p, ρ_f, g are density of particles, gasifying agent and gravitational force respectively.

By balancing net weight of particles and upward force

$$\Delta P = (1 - \epsilon) \times (\rho_p - \rho_f) L \times g$$

Using the value of pressure drop ΔP in equation (4)

$$1.75 D_p \rho_f {V_{mf}}^2 + 150(1 - \varepsilon)\mu V_{mf} = (\rho_p - \rho_f) {D_p}^2 g \varepsilon^3 \quad (5)$$

At the balancing point of total bed weight and upward force the superficial gas velocity (V_s) is referred as minimum fluidization velocity (V_{mf}).

2.5.3 Void Fraction

Packing characteristics are required to understand the design and operation of a packed bed. During our experiment the bed is made densely packed. After pouring the particles into the bed and shaking it for several minutes the bed is made densely packed. Several authors ranged the voidage 0.37 to 0.39 for dense packed bed of monosized spherical particles (13).

For complexity of defining the voidage for non-spherical particles, very little theoretical and experimental work has been performed. It is suggested by Brown in 1966 (13), packing void fraction depends on particles sphericity and based on his experiment it has shown the voidage can relate to the sphericity as below table.

Table 2.1: Voidage of Randomly Packed Beds with uniformly sized Particles Larger than 500 μm. (Packing of Non-Spherical particles) (13)

	Voidage	
Sphericity	Loose Packing	Dense Packing
0.25	0.85	0.8
0.3	0.8	0.75
0.35	0.75	0.7
0.4	0.72	0.67
0.45	0.68	0.63
0.5	0.64	0.59
0.55	0.61	0.55
0.6	0.58	0.51
0.65	0.55	0.48
0.7	0.53	0.45
0.75	0.51	0.42
0.8	0.49	0.4
0.85	0.47	0.38
0.9	0.45	0.36
0.95	0.43	0.34
1	0.41	0.32

2.5.4 Hydrodynamics Behavior of Fluidized Bed

Operation of fluidized bed has many applications in industry and for this reason many works have been found in literature. In industrial application bed diameter, particles size, particles shapes, bed height play very important rule. Many works based on particles size, bed diameter, bed height, particles shape have found in literature also.

In a cylindrical shape fluidized bed, the effect of particles diameter and bed height on minimum fluidization velocity was investigated by Gunn et al. (20). They found no significant effect on minimum fluidization velocity for bed height. Both rectangular bed (2D) and cylindrical bed (3D) was used by Geldart el al. ((21). Six different bed heights were used for both 2D and 3D fluidized bed and it has been found that there is no effect on minimum fluidization velocity on increasing bed height for cylindrical fluidized bed. On the other hand, minimum fluidization velocity increased for increased bed height for rectangular shape fluidized bed. Two fluidized bed with different diameter size (0.29 m and 0.089 m) were investigated by Hilal et al. (22) and they found decreased minimum fluidization velocity with increased bed diameter. A rectangular fluidized bed with 1×0.2×0.012 m dimension and a range of particles from 160-700 μm was used by Ramos et al. (23). They used different bed height and bed widths and concluded their investigation that minimum fluidization velocity decrease with increased bed width and increase with increased bed height and particles diameter. Geldart Type-D particles were used with different bed height in a 300×300 mm shape rectangular fluidized bed by Zhong el al. (24). They also concluded increasing minimum fluidization velocity with increasing 2D bed size. A conical tapered fluidized bed with various bed heights was investigated by Sau et al. (25). Their investigation found no significant effect on minimum fluidization velocity with increasing bed height for tapered fluidized bed but minimum fluidization velocity increase with increasing tapered angle. Zhon et al. (26) investigated a 0.4×0.4 m rectangular bed with chips, mung, beans, millet, corn stalks and cotton stalks to study the effect of particles size, shape and density on minimum fluidization velocity. Their investigation concluded increasing minimum fluidization velocities with increasing length to diameter ratio of fluidized bed. Two fluidized bed column with 1.6 and 2.4 cm diameter were investigated by Rao et al. (27). Glass beads (100-600μm) with 2500 kg/m^3 and polystyrene beads (250-354μm) with 1250 kg/m^3 were used in their investigation. They found in their investigation that minimum fluidization velocity

influenced by bed diameter and minimum fluidization velocity increase with reducing bed diameter. The effect of bed height and material density on minimum fluidization velocity in a cylindrical bed with glass beads, ground corncob and ground walnut shells at different bed heights was investigated by Escudero et al. (28). Their investigation found that each type of particle has no influence in minimum fluidization velocity with increasing height and minimum fluidization velocity influenced by particles density. It increases with increase of particle density.

Chapter 3: Experimental Setup & Technical Approach

This chapter will clearly describe about the laboratory scale fluidized bed system with its different apparatus to study the hydrodynamics of gas-solid fluidized bed system. Experimental procedure, technical approach and theoretical considerations are also presented in this chapter. Section 3.1 describes the design parameter of 12.4 cm diameter fluidized bed reactor and air supply, control procedures. Section 3.2 describe about test particles selection, preparation and different parameter of particles. Section 3.3 describes about experimental measurement procedures. Section 3.4 describes the method of high speed flow visualization. Section 3.5 and 3.6 describes about test matrix and statistical analysis of experimental measured data respectively.

3.1 EXPERIMENTAL SETUP

Figure 3.1 shows the schematic diagram of our laboratory scale fluidized bed. From figure it has been shown that a high-pressure blower with 3730 KW and 34 m^3/min flow rate has been used to supply gasifying agent (air) to the test section. The air was supplied to the test section by 300 cm long and 12.7 cm diameter sheet metal pipe with three elbows.

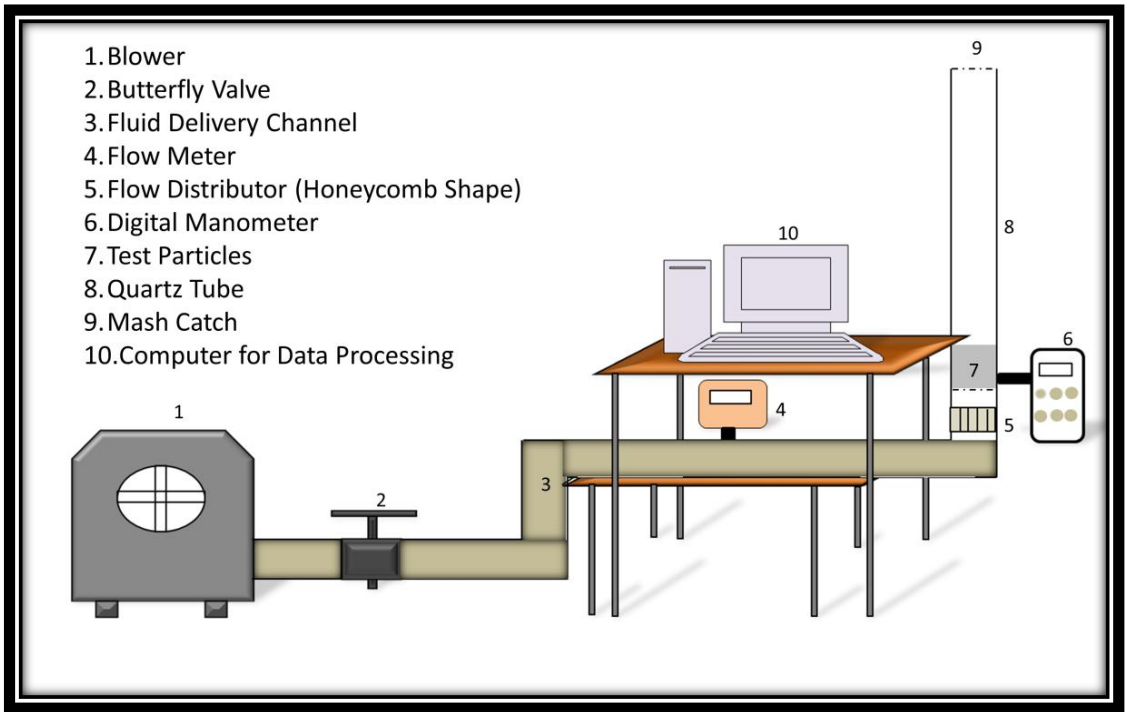

Figure 3.1: Schematic Diagram of Laboratory Scale Fluidized Bed

This length and elbows were used the meet the requirement of using flow meter which was recommended by flow meter manufacturer to get the proper flow rate reading through the cross section of sheet metal pipe. The blower has a rectangular shape outlet. For this reason a duct reducer with 12.7 × 17.8 cm rectangular to 10.2 cm circular duct was used and connected from blower outlet to sheet metal pipe inlet. To control the flow rate to the test section a wafer style butterfly valve with 12.7 cm diameter and 5.7 cm thickness was used and connected between the blower and first elbow among three. This butterfly control valve was rated for 200 PSI. For measuring flow rate across the bed a thermal mass flow meter was used between second and third elbow. Distance between elbows and flow meter was maintained as flow meter manufacturer requirement.

The bottom part of test section was by made of plexi glass tube with 12.7 cm outer diameter and 3.18 m wall thickness. Also a quartz tube with 12 cm outer diameter and 0.318 cm wall thickness was inserted into plexi glass tube. This quartz tube will assist to attain better optical access for particle image velocimetry (PIV) and also for shadow sizing analysis for dilute part of test section during experiment.

A mesh made of brass with 53 micron was installed into test section to hold particles. Another mash with same type was also installed at top part of bed column section to hold the particle from falling out of the bed column. To measure the pressure drop across the bed a small opening was made at 1.5 cm above from bottom of test section. A tygon tube from digital manometer was connected to that small opening. Also a small part of mesh with 53 micron was attached to that small opening to restrain the particle entering into tube. For uniform distribution of gasifying agent (air) to the test section a honeycomb shape distributor was inserted 8 cm below from test section. An external power supply was used for thermal mass flow meter.

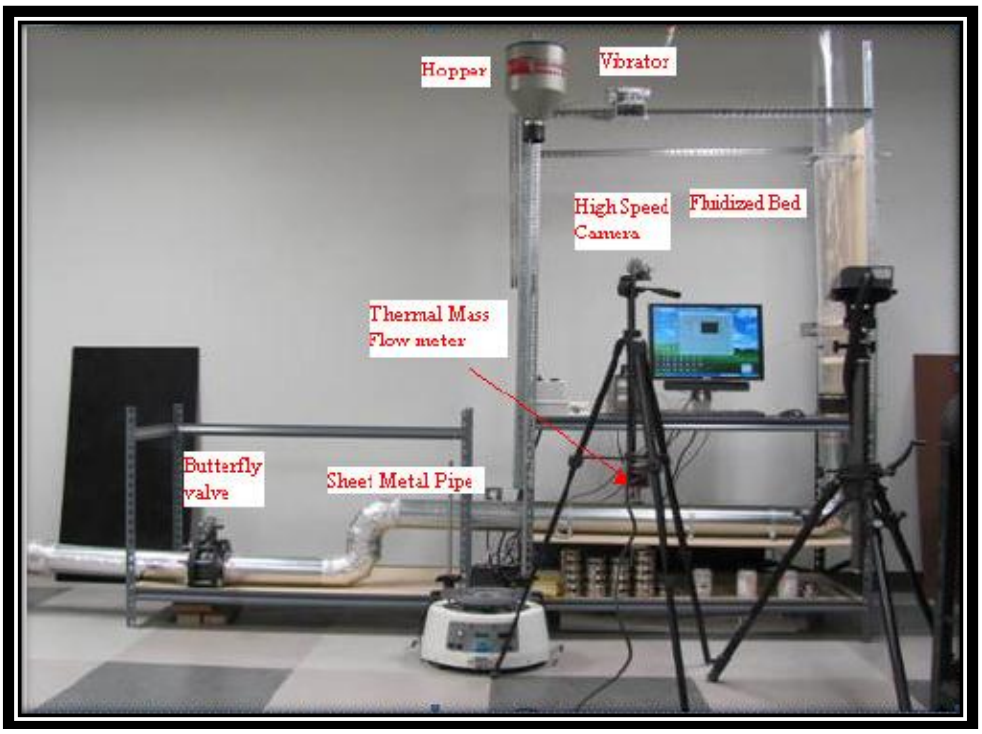

Figure 3.2: Laboratory Scale Fluidized Bed

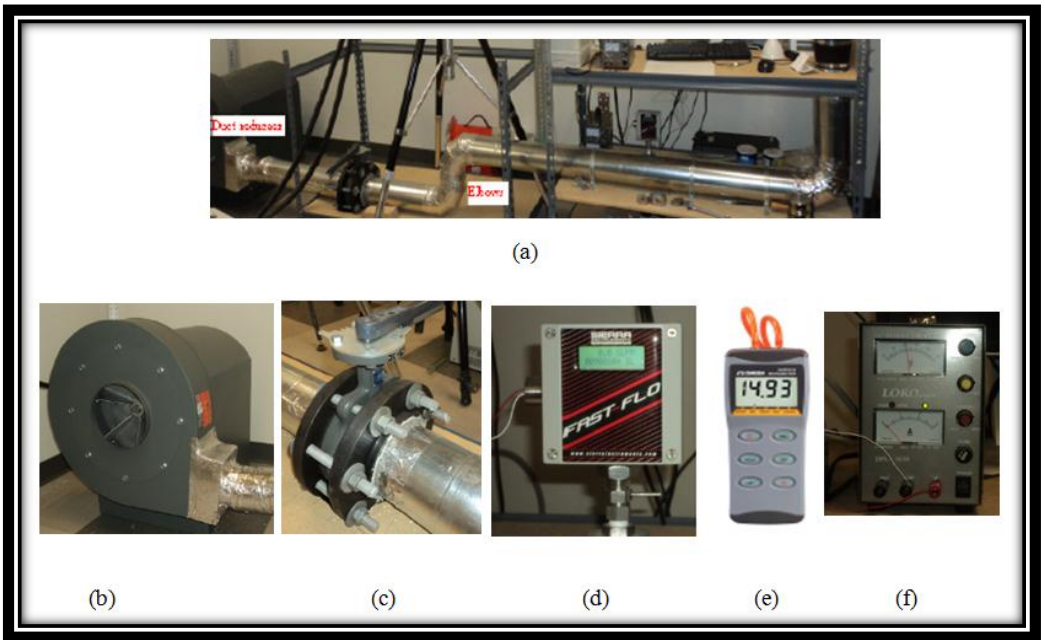

Figure 3.3: Air Delivery System (b) High Pressure Blower (c) Butterfly Valve (d) Thermal Mass Flow Meter (e) Digital Differential Manometer (d) External Power Supply

3.1.1 Previous Experimental Setup

Before laboratory scale fluidized bed a pilot scale fluidized bed was made with 3.8 cm outer diameter, 0.318 cm wall thickness and 183 cm height. Our current experimental set up has quartz tube bed column with 0.124 m inner diameter. Experimental data of both setups will compared in result section and will find out the effect of bed column diameter. Same test materials were used for both setups. Figure 3.4 shows the pilot scale fluidized bed with 3.8 cm outer thickness.

Figure 3.4: Pilot Scale Fluidized Bed

3.2 TEST MATERIAL

To investigate fluidized bed internal hydrodynamics and bed behavior borosilicate glass beads with density 2230 kg/m^3 was selected as test material. Spherical and non-spherical shape of glass beads were selected for experiment. In many cases investigation on laboratory scale fluidized bed spherical

particles were chosen. But in real coal gasification plant, coal particles are non-spherical. In our experiment we selected both spherical and non-spherical particles.

For spherical 1 mm borosilicate glass beads were chosen with density 2230 kg/m^3. Figure 3.5 shows sample image of spherical particles.

Figure 3.5: Zoomed Image of 1 mm Spherical Particles.

3.2.1 Production of Non-Spherical Particles

To produce non spherical particles 6 mm borosilicate glass beads were crashed by a CRAVER 3851 hydraulic compressor. A die and punch system with 5.08 cm diameter was used to put the spherical particles and then crushed into hydraulic compressor. This stainless steel die and punch was capable to withstand high pressure exerted by hydraulic compressor.

Crushed particles contained different ranges from few microns to large irregular shape. Crushed large particles were crushed again to get required size as our experimental requirement. To categorize these crushed particles an Octagon digital with 60 Hz, 110 volts, single phase sieve shaker was used with mounting different sieve plate into the sieve shaker to get desired particle size distribution. Ranges of sieve plates were 20$\mu m$to 2000μm. To measure the particle weight a precision weighing balance was used with capacity 620g and readability 0.001 g.

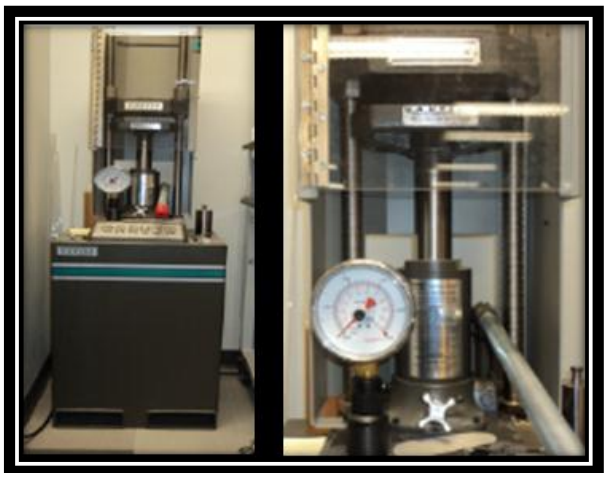

Figure 3.6: CRAVER 3851 Hydraulic Compressor

3.2.2 Measurement of Particle Size and Shape

There are many industrial applications of aggregate particle materials. To get optimum operation process, measurement of particle size and shape is important.

For grading aggregate particles distribution most widely used method is mechanical sieving technology. Sieving method divides the aggregate particles into fractions where each fraction contains a certain rage of particle size. (29)

At first the sieves are arranged by putting them one after another from lower range to higher range. At bottom a pan was placed to hold the powder like particles. After that the staked sieve placed into sieve shaker. Sample of aggregate particles put into top larger sieve pan and covered. Sieve shacking was carried out for specific period of time. Particles pass gradually from larger sieve aperture to lower sieve aperture. Finally, fraction of particles from each sieve was weighing by a precision balance with capacity 620 gm. and readability 0.001 gm.

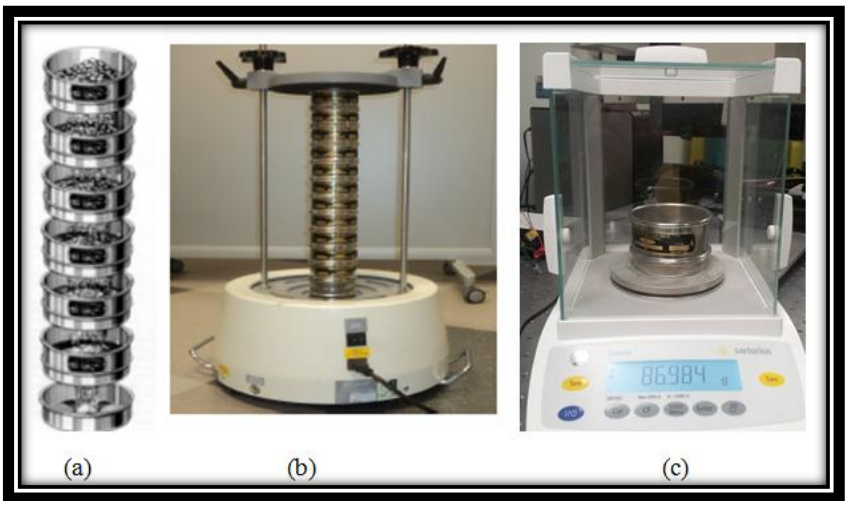

Figure 3.7: (a) Stake of Sieve Pan (b) Sieve Shaker (c) Precision Balance

3.2.3 Sphericity Measurement

Digital Image Processing (DIP) has widespread application in medicine, biology, geography, meteorology, manufacturing, material science. Also for particulate technology, size and shape analysis is very important. Beyond the recent use of DIP technology it can also be used for size and shape analysis. (29). Motivated by these applications, instead of processing the digital image we used to take digital image and find out the larger circumscribe circle of the particle by using software provided with DinoLite, the versatile digital microscope.

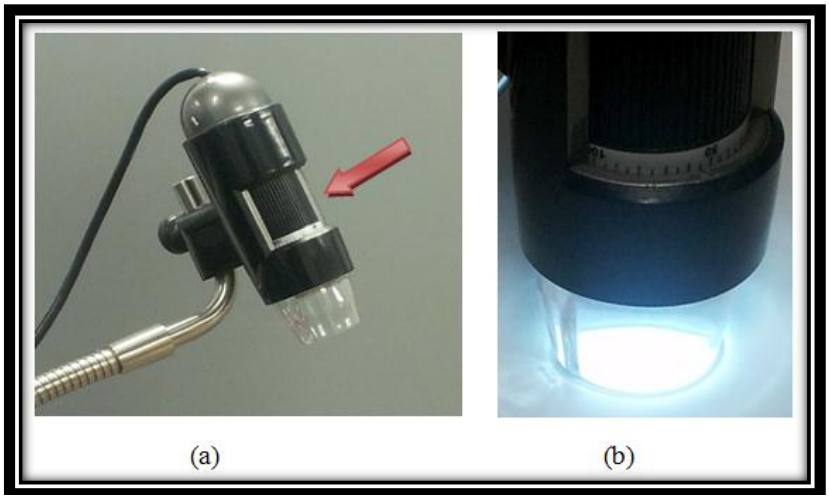

Figure 3.8: (a) Dino Capture Microscope (b) Focusing the Particles

At first the object was focused by adjusting the dial with microscope and then the image was captured. While adjusting the dial, the dial number (magnification value) was noted and put into with magnification window before play with the image to get circumscribe diameter of the particle. Before measure the circumscribe diameter of particle standard measurement ruler was used to calibrate the Dino Captured Microscope.

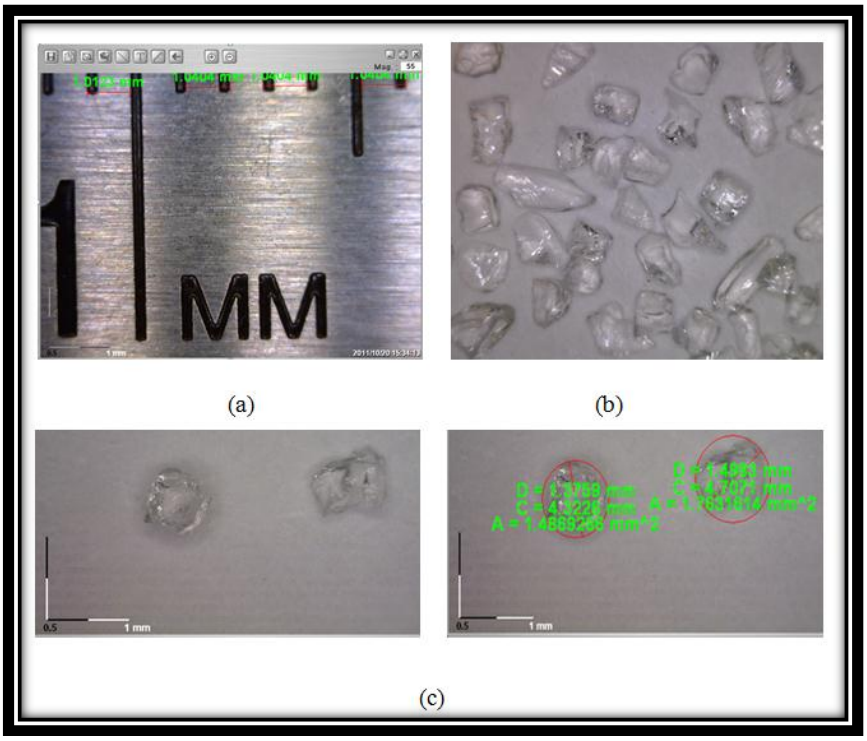

Fig 3.9: (a) Calibration Image (b) Sample Image of Non-Spherical Particle (c) Measurement of Circumscribe Diameter of Non-Spherical Particles

W.C. Krumbein (30) describes the expression for sphericity of made by Hakon Wadell (31) . According to Wadell definition sphericity (φ) is as follows,

$$\varphi = \sqrt[3]{\frac{Volume\ of\ Particle}{Volume\ of\ the\ Circumscribe\ Sphere}}$$

Here from Wadell expression, particle volume has the same volume in terms of sphere and the diameter is the nominal diameter of the particle (d). From this expression the basic volume of particle is$\frac{\pi}{6}d^3$. In general, the volume of circumscribe sphere has the longest diameter (a) of the particle, so the volume of circumscribe sphere is$\frac{\pi}{6}a^3$. From these values the Wadell expression for sphericity comes as follows,

$$\varphi = \sqrt[3]{\frac{Volume\ of\ Particle}{Volume\ of\ the\ Circumscribe\ Sphere}} = \frac{\frac{\pi}{6}d^3}{\frac{\pi}{6}a^3} = \frac{d}{a}$$

Krumbein used this expression to measure the sphericity of particle where the sphericity is the ratio of nominal diameter and longest diameter of the particle. Krumbein used to measure the longest diameter of particles with slide calipers.

As our test particles are crushed and they have the size of micro level, we used the digital image technology to get the longest diameter of the particles (a) and the nominal diameter was considered as the mean sieve diameter (d).

For our project work, to investigate the effect of particle size in fluidized bed we accumulate different ranges of particles. The ranges of test particle are mentioned in test matrix section 3.5.

Sphericity was measured for each particle ranges between 500-2000 micrometer by random selection and the sphericity was found between 0.45 and 0.93. It is also found that mean sphericity of crushed glass particles is 0.65 (Table 2) (13)

Table 3.1: Sphericity of Different Shapes, Materials and Commonly Used Packings (13).

Types of Particles	Sphericity
Sphere	1.00
Cube	0.81
Cylinder	
h=d	0.87
h=5d	0.70
h=10d	0.58
Disks	
h=d/3	0.76
h=d/6	0.60
h=d/10	0.47
Activated Carbon and	0.70-0.90
Coal	0.63-0.73
Cork	0.69
Glass, Crushed, Jagged	0.65
Sand	0.86-0.53
Wheat	0.85
Tungsten Powder	0.89

3.3 BED PRESSURE DROP AND FLOW RATE MEASUREMENT

A digital manometer capable for measuring differential pressure and also positive or negative gauge pressure was used. To measure bed pressure drop differential pressure option was selected. A tygon tube with 5 mm inner diameter was connected from manometer to small opening in fluidized bed. This small opening was at 1.5 cm above from bottom of fluidized bed. A mash catch with 53 micron was attached to the opening to protect tube and manometer from entering test particles during experiment. Figure 3.10 shows pressure measurement port connected with digital manometer. This manometer is capable of measuring between 0-2 psi pressure drop.

Test particles were prepared by adding static guard before experiment. Static guard was used to remove inter particles bonding. Test particles were poured into bed from top opening of bed column and then bed column was shacked for several times. This shaking helps particles get packed. Before starting experiment it was observed to remove loosened particles. The bed was shacked again and again if required.

The experiment was to measure bed pressure drop along with increasing flow rate of gasifying agent (air). Flow rate was also measured at the same time. The air flow rate was increased gradually by regulating butterfly valve up to separation starts in test particles. This is the point of minimum fluidization. Air flow rate and pressure drop was measured at this point and compared for different bed height and different size of test particles. At the point of minimum fluidization a small bed height increasing observed by high speed imaging. This increasing bed height will describe in high speed visualization section. After minimum fluidization, flow rate was increased until they trapped into top mash which is connected into top part of bed column. The particles are entrained and reach the terminal velocity. By this time fluidized bed has undergone different fluidization regimes describe in section 2.4.2.

Figure 3.10: Digital Manometer with RS 232 Cable

Measured value of differential pressure drop was feed into Handheld Data Logger (Figure 3.11) by RS 232 cable. Both manometer and data logger gives the pressure drop reading up to 3 decimal point with ±0.3% accuracy.

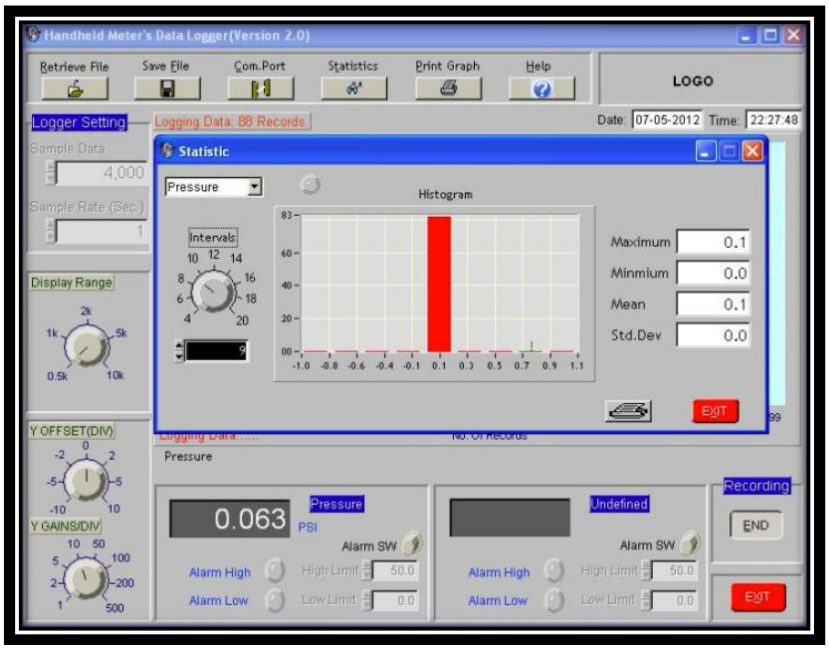

Figure 3.11: Handheld Data Logger for Digital Manometer

At the same time mass flow was measured by insertion type mass flow meter with 200 milliseconds response. The flow meter is shown in figure 3.3 (d) which was used to measure volumetric flow rate. This flow meter was also factory calibrated to range of 0 to 4000 SLPM. An external power supply with 20 VDC was also used to run the flow meter. Data from flow meter was feed into Sierra

Smart Interface software provided by flow meter manufacturer. Figure 3.12 shows data logger for flow meter.

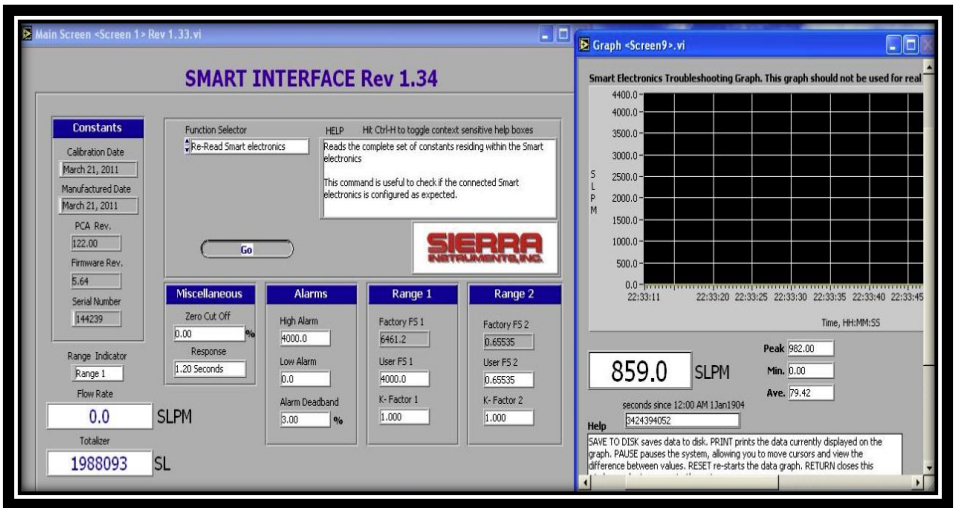

Figure 3.12: Data Logger for Flow Meter

3.4 HIGH SPEED FLOW VISUALIZATION

In chemical engineering like combustion process, mineral processing, pharmaceutical production concentrated gas-solid multiphase flows plays an important role. Numerous investigations observed due to importance of multiphase flow with their complicated flow structures (32).

In our current experiment an attempt has taken to observe the flow structure in dilute section while the fluidized bed is fully fluidized. 210 mm above from the top surface of test particles (5.5 cm bed height) was considered as the test section. Also just after the top surface of test particles was considered as test section. At this section collapsing of bubbles were visible. Both spherical and non-spherical particles (1 mm nominal diameter) were taken as test particles.

To get particles velocity and particle size the Dynamic Studio Shadow Sizer measurement technique was used. By using backlit and shadow image analysis software this technology can measure size, shape, and velocity including wide range of particle types like bubbles, liquid droplets, solid particles and particles with well-defined contour (33).

3.4.1 Shadow Sizing Measurement Principle

A camera and a light source are required for shadow sizing. A ground glass diffuser plate is also placed between the light source and the test section. This ground glass diffuser helps to take the images of test particles as a shadow. Figure 3.13 shows the schematic diagram of shadow sizing technology.

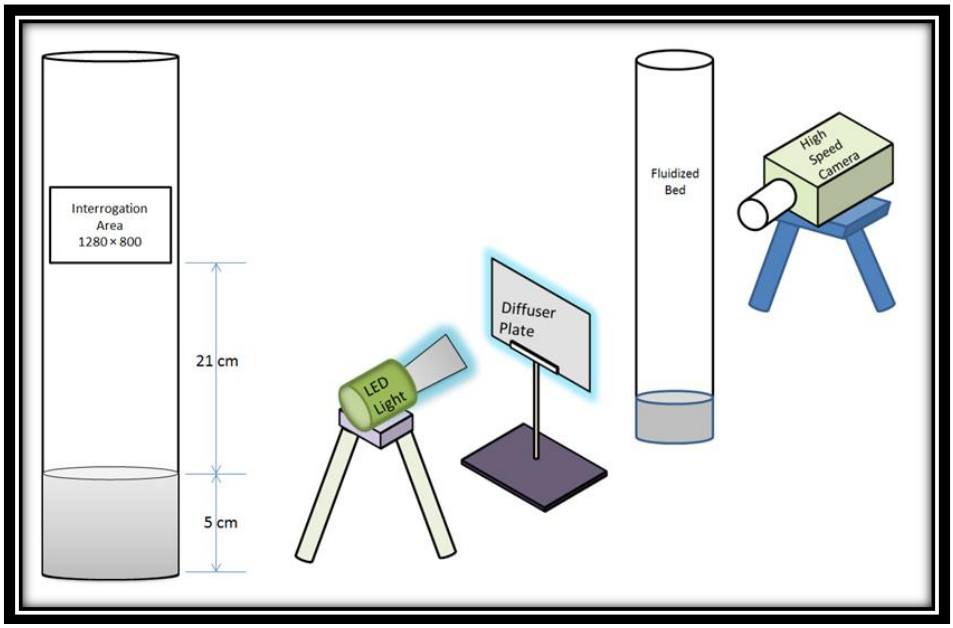

Figure 3.13: Schematic Diagram of Shadow Sizing

For light source LED based honeycomb and constellation illuminator was used with delivering lower to higher luminosity as required to get a perfect shadow image of test section. Figure 3.14 shows the LED based light source.

Figure 3.14: LED Constellation System

To capture the image a Phantom high speed camera with 5 KHz was used. Image triggering rate can be change by using dynamic studio software. For the current experiment all the images have taken with 1000 Hz. Figure 3.15 shows the Dantec high speed camera.

Figure 3.15: Dantec High Speed Camera

Both camera and LED light source are synchronized by a timer box. While the particles flows through the test section a light flash acquires and at the same time camera capture the image with help of synchronization device and freeze the particles motions. After acquiring the images shadow sizing software use advanced edge detection algorithm to detect the particles and their shape. To find out the velocity shadow sizing uses two consecutive images with very short interval and particle tracking algorithm.

Figure 3.16: Shadow Sizing

Again without using the backlit light source (LED light) only high speed camera was used to visualize the fluidized bed test particles behavior. Two state of fluidization were observed for both spherical and non-spherical particles. 1) Incipient of minimum fluidization. 2) Bubbling Fluidization. These two observations will give a fundamental idea about particles behavior for a respective flow velocity of gasifying agent (air).

3.4.2 Calibration

Before processing the images it is required to capture a calibration image. A scale factor should measure from that calibration image. Images taken by high speed camera is in pixel unit. To get physical parameter of particles and their velocities in metric unit it is required to convert image from pixel unit to metric unit. A ruler scale is placed in test section and calibration image was taken. From measure scale factor window in dynamic studio software two points were selected and their numeric distance was put as required in metric unit. Figure 3.17 shows a calibration image taken from dynamic studio software.

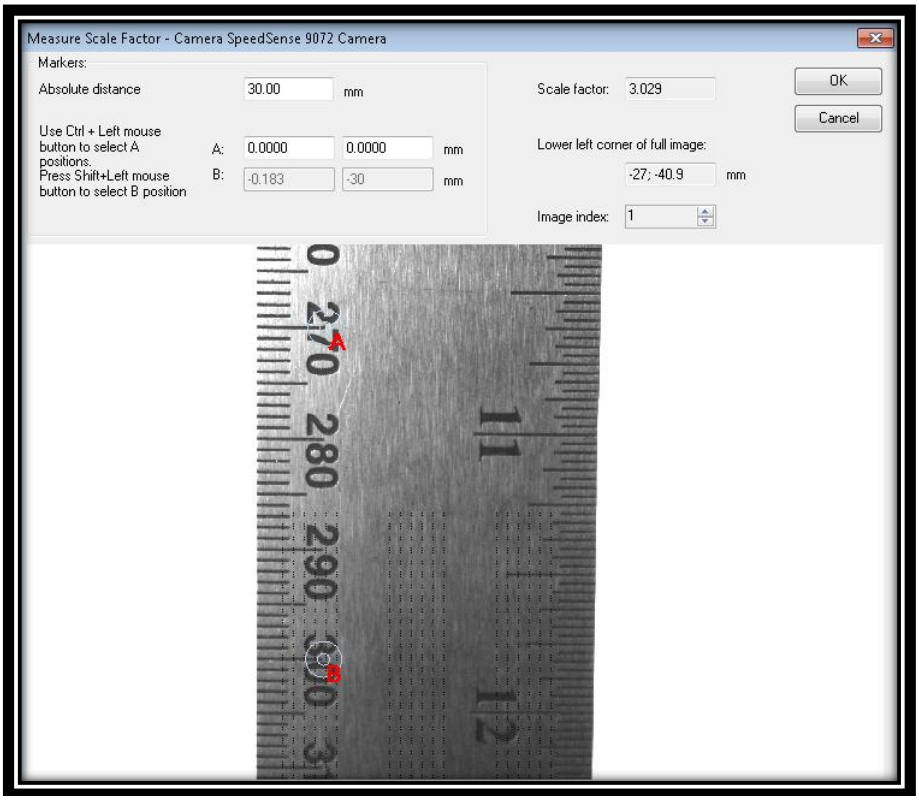

Figure 3.17: Calibration Image

3.4.3 Shadow Sizer Processing

According to shadow principle shadow sizer processing acquires data of particle size, shape, velocity, their position. Because of shadow principle there is no limitation of particle size and shape (33).

Images were taken from test section with single frame and 1000 Hz. Later single frame images were converted into double frame images. Double frame images were required to get particles velocity. From particles characterization window shadow assistant helps to capture the particle from the image. Particle was selected by shadow assistant with their contour and statistical information like particle pixel depth and edge gradients. Figure 3.18 shows a selection method of particle with the help of shadow assistant.

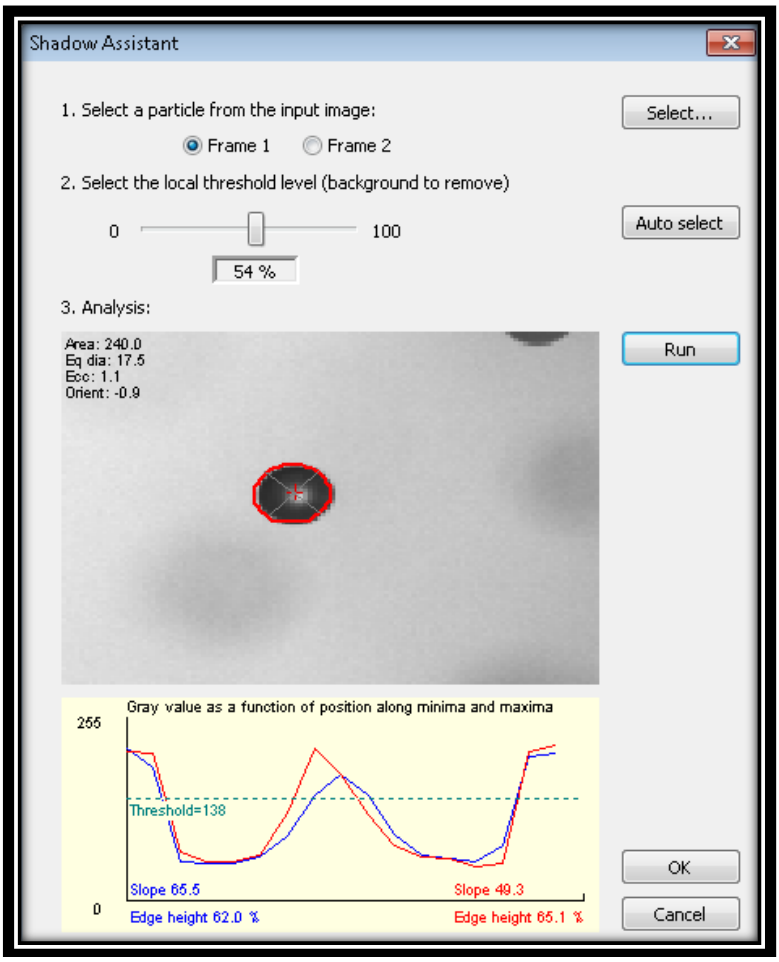

Figure 3.18: Particle Selection with its Contour

After shadow sizer processing it can detect the particles, their contour, their velocity with direction and also their mean diameter. Figure 3.19 shows a sample of double frame image and figure 3.20 shows its shadow processed results.

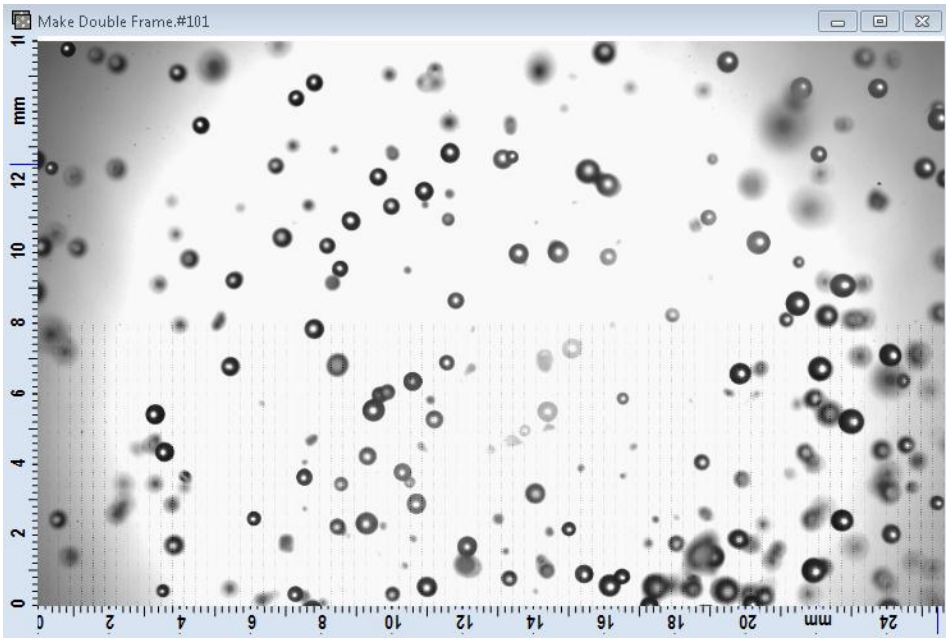

Figure 3.19: Shadow Image of Test Particles

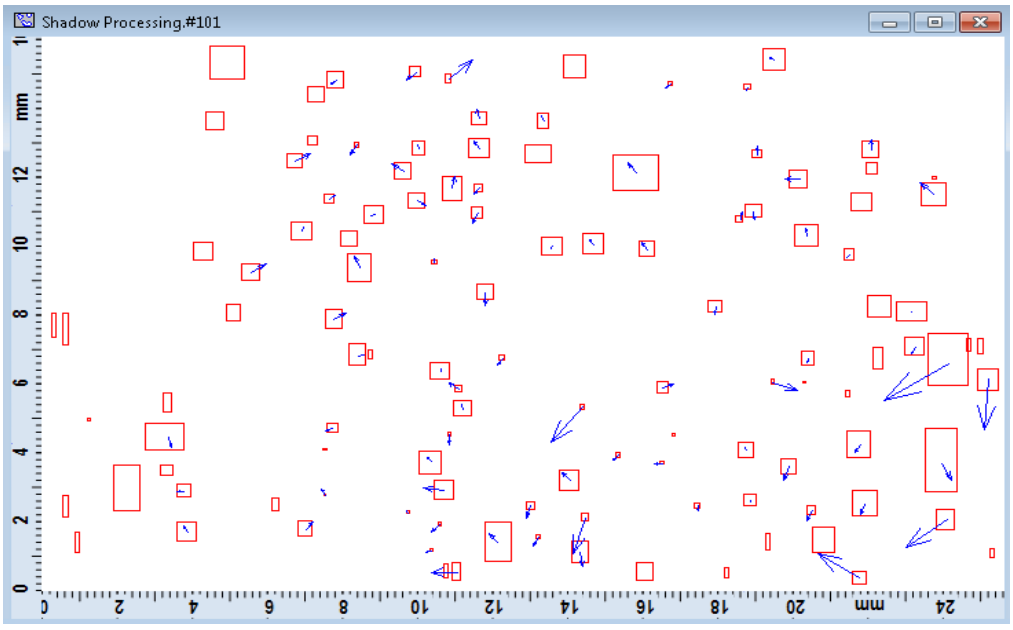

Figure 3.20: Example of Shadow Sizer Processed Result

3.5 TEXT MATRIX

To accomplish our experiments many initiative has taken and a brief description our test matrix is presented here below.

Test objectives:

1) Hydrodynamics behavior of fluidized bed with spherical and non-spherical particles
2) High speed flow visualization for spherical and non-spherical particles at incipient fluidization and bubbling fluidization regimes
3) Flow field visualization for spherical and non-spherical particles with shadowgraphy.

A test matrix has shown below of our experiment to observe hydrodynamics of laboratory fluidized bed.

Table 3.2: Test Matrix to Observe Bed Hydrodynamics

Fluidized Bed	Particle	Particle Size (mm)	Bed Height (cm)
12.4 cm Bed Diameter	Spherical	1.0 mm	2.0, 2.5, 3.0, 4.0, 5.0, 5.5, 6.0, 6.5, 7.0
	Non-Spherical	1.0-1.18	2.5, 3.0, 4.0, 5.0, 5.5
		0.85-1.0	2.5, 3.0, 4.0, 5.0, 5.5
		0.85-1.18	2.0, 2.5, 3.0, 4.0, 5.0, 5.5
		0.71-0.85	3.0, 4.0, 5.0, 5.5
		0.6-0.71	3.0, 4.0, 5.0, 5.5
		0.50-0.60	3.0, 4.0, 4.5
		0.355-0.50	3.0, 4.0, 5.0, 5.5
		0.155-0.355	3.0, 4.0, 5.0, 5.5
3.5 cm Bed Diameter	Spherical	1.0 mm	3.0, 5.0

Table 3.3: Test Matrix for High Speed Flow Visualization

Particle Size (mm)	Shape	Fluidization State
1.0	Spherical	Incipient & Bubbling Fluidization
0.85-1.0	Non-Spherical	
0.355-0.50		

Table 3.4: Test Matrix for Shadowgraphy

Particle Size (mm)	Shape	Fluidization State
1.0	Spherical	Full Fluidization & Bubbling Fluidization
0.85-1.18	Non-Spherical	
0.355-0.50		
0.155-0.355		

3.6 STATISTICAL ANALYSIS OF EXPERIMENTAL DATA

For experimental results it is required to identify the specifications for measuring systems. While taking measurement it is observed some randomness into measured data even if the same measurement has taken repeatedly. This randomness mainly caused by uncontrolled variables, less precision of measuring instrument. This randomness can make an effect on drawing a conclusion from measured data (34). Thus, before using experimental data it is obvious to make a statistical analysis of those. Table 3.4 shows 29 data set of pressure drop (unit=Pa) taken with constant flow velocity .073 m/sec.

Table 3.4: Experimental data set of pressure drop at 0.73 m/sec flow velocity

506.07342	499.8682	503.3155	515.726	515.726	511.5892
512.27868	494.3524	509.5208	494.4903	510.8997	516.4155
496.42079	516.4155	506.7629	512.9682	517.7945	528.1366
502.62605	499.1787	508.1418	499.1787	512.2787	507.4524
507.45237	515.726	499.8682	526.0681	529.5155	

These measurements were taken for non-spherical particles ranges from 355-500 μm. 1 minute interval were taken before taking each data. Basic statistics of measured data has shown in table 3.5

Table 3.5: Statistical Description of Measured Data

Number of Measured Data	Minimum Value	Maximum Value	Mean Value	Median	Standard Deviation
29	494.35	529.52	509.53	509.52	9.4

From statistical analysis it is found that standard deviation is 9.4 Pa. Standard deviations are considered as statistically significant – normal random error (35). Because of some error in measurement a constant value is always needed to add up to the measured value. That added value was 6.89 Pa. This value is referred as bias error. Table 3.6 shows a statistical analysis of measured data.

Table 3.6: Statistical Analysis of Pressure Drop with .073 m/sec Flow Velocity

Mean Pressure	Random Error	Bias Error
509.53 Pa	9.40 Pa	6.89 Pa
Error in Percentage	1.84%	1.35%

On the other hand figure 21 shows a statistical histogram of pressure drop with din width range 5 Pa.

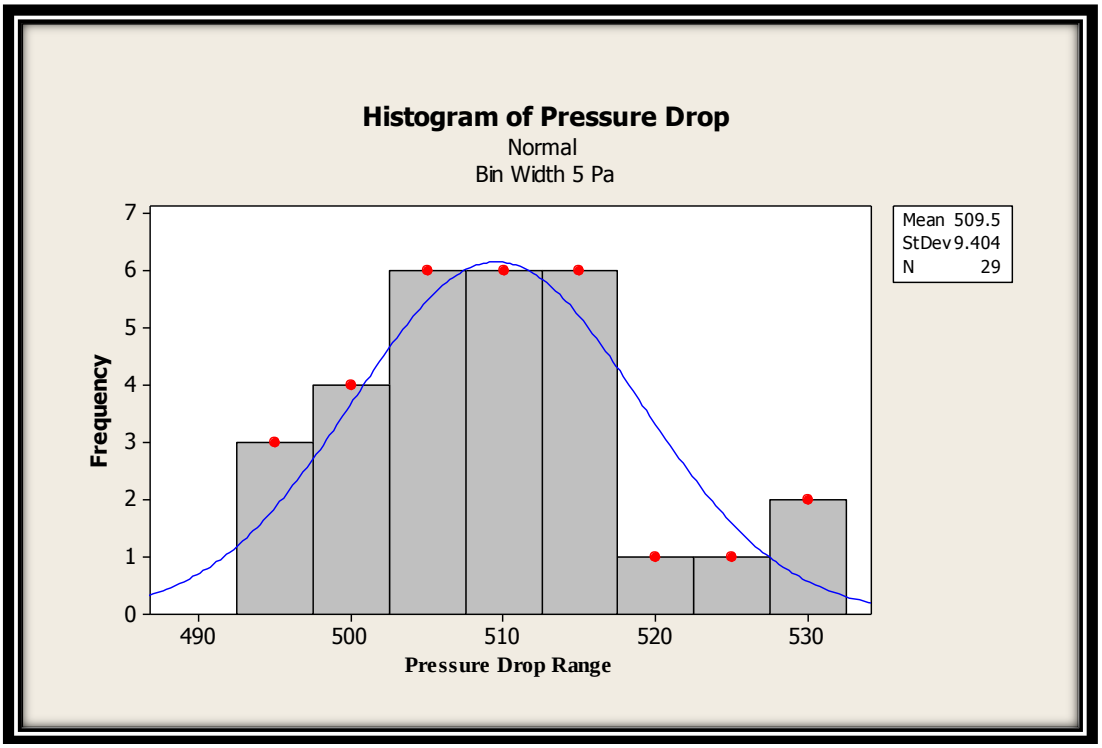

Figure 3.21: Histogram of Pressure Drop

95 % Confidence interval was also calculated by using t-distribution table (Figure 3.22). Form our measured data the degree of freedom is 28. For 95% confidence interval and for degree of freedom 28 our required value from t-distribution table is 2.048. Finally, from standard procedure our lower and upper ranges were found. The ranges are 505.47 to 513.09.

df	a = 0.1	0.05	0.025	0.01	0.005	0.001	0.0005
∞	t_s = 1.282	1.645	1.960	2.326	2.576	3.091	3.291
1	3.078	6.314	12.706	31.821	63.656	318.289	636.578
2	1.886	2.920	4.303	6.965	9.925	22.328	31.600
3	1.638	2.353	3.182	4.541	5.841	10.214	12.924
4	1.533	2.132	2.776	3.747	4.604	7.173	8.610
5	1.476	2.015	2.571	3.365	4.032	5.894	6.869
6	1.440	1.943	2.447	3.143	3.707	5.208	5.959
7	1.415	1.895	2.365	2.998	3.499	4.785	5.408
8	1.397	1.860	2.306	2.896	3.355	4.501	5.041
9	1.383	1.833	2.262	2.821	3.250	4.297	4.781
10	1.372	1.812	2.228	2.764	3.169	4.144	4.587
11	1.363	1.796	2.201	2.718	3.106	4.025	4.437
12	1.356	1.782	2.179	2.681	3.055	3.930	4.318
13	1.350	1.771	2.160	2.650	3.012	3.852	4.221
14	1.345	1.761	2.145	2.624	2.977	3.787	4.140
15	1.341	1.753	2.131	2.602	2.947	3.733	4.073
16	1.337	1.746	2.120	2.583	2.921	3.686	4.015
17	1.333	1.740	2.110	2.567	2.898	3.646	3.965
18	1.330	1.734	2.101	2.552	2.878	3.610	3.922
19	1.328	1.729	2.093	2.539	2.861	3.579	3.883
20	1.325	1.725	2.086	2.528	2.845	3.552	3.850
21	1.323	1.721	2.080	2.518	2.831	3.527	3.819
22	1.321	1.717	2.074	2.508	2.819	3.505	3.792
23	1.319	1.714	2.069	2.500	2.807	3.485	3.768
24	1.318	1.711	2.064	2.492	2.797	3.467	3.745
25	1.316	1.708	2.060	2.485	2.787	3.450	3.725
26	1.315	1.706	2.056	2.479	2.779	3.435	3.707
27	1.314	1.703	2.052	2.473	2.771	3.421	3.689
28	1.313	1.701	2.048	2.467	2.763	3.408	3.674
29	1.311	1.699	2.045	2.462	2.756	3.396	3.660
30	1.310	1.697	2.042	2.457	2.750	3.385	3.646
60	1.296	1.671	2.000	2.390	2.660	3.232	3.460

Figure 3.22: t-distribution table (36)

Chapter 4: Results and Discussions

This section presents experimental results of hydrodynamic behavior of bed for spherical and non-spherical particles. Also high speed flow visualization at different flow regimes and flow field visualization using shadow sizing technology.

Minimum fluidization velocity and bed pressure drop are the most important parameters to characterize fluidized bed. From experimental results of hydrodynamic behavior the following section has described which has the effect on minimum fluidization velocity and bed pressure drop.

1) Effect of bed height for spherical and non-spherical particles.
2) Effect of bed diameter for spherical and non-spherical particles.
3) Effect of particle shape on minimum fluidization

On the other hand visualization at two fluidization regimes also observed with high speed camera. At the state of incipient minimum fluidization and bubbling fluidization regimes this high speed visualization has observed for both spherical and non-spherical particles. Again to observed flow field at full fluidization region for both spherical and non-spherical particles with different size was also observed with shadow sizing technology. Shadow sizing technology has described in section 3.4.

4.1 EFFECT OF BED HEIGHT FOR SPHERICAL PARTICLES

Pressure drop and minimum fluidization velocity were measured across the bed with increasing superficial gas velocity. Spherical and non-spherical test particles with 1 mm nominal diameter were used to observe the effect of bed height. Figure 4.1 shows effect of bed height from 3 to 6 cm for spherical particles for 12.4 cm bed diameter.

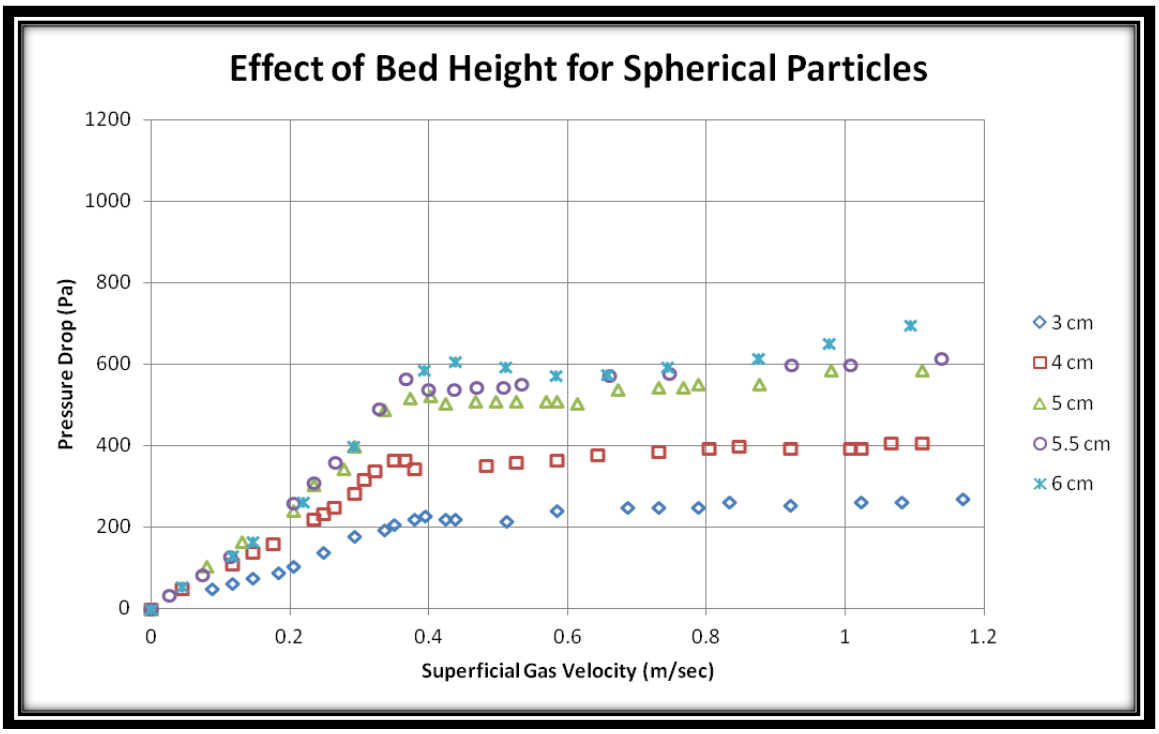

Figure 4.1: Effect of Bed Height for Spherical Particles

Table 4.1: Analytical and Experimental Pressure Drop for 1 mm Spherical Particles

Bed Height (cm)	Analytical Minimum Fluidization Velocity,(m/sec)	Experimental Minimum Fluidization Velocity, Vs (m/sec)	Analytical Pressure Drop (Pa)	Experimental Pressure Drop (Pa)	Deviation in Pressure Drop	Ratio of Bed Height and Bed Diameter (H/D)
2.00	0.40	0.42	273.24	130.00	52.42%	0.16
2.50	0.40	0.40	341.53	193.00	43.49%	0.20
3.00	0.40	0.39	409.83	227.52	44.48%	0.24
4.00	0.40	0.36	546.44	365.42	33.13%	0.32
5.00	0.40	0.40	683.00	524.00	23.28%	0.40
5.50	0.40	0.40	751.36	565.36	24.76%	0.44
6.00	0.40	0.43	819.00	606.00	26.01%	0.48
6.50	0.40	0.36	887.00	682.00	23.11%	0.52
7.00	0.40	0.40	956.00	737.00	22.91%	0.56

Analytical pressure drop was calculated from Ergun equation (eq^n 4) which is a function of particle diameter, bed height, superficial gas velocity, particle density, gas density and void fraction. Table 4.1 shows the list of analytical and experimental measurement of pressure drop for different height ranges from 2 to 7 cm. Comparatively large deviation between analytical and experimental pressure drop found in 2 cm bed height. This deviation gradually decreases with the increase of bed height. On other way it can be say that while the ratio of bed height and bed diameter (H/D) increases

the deviation between analytical and experimental pressure drop decreases. Moreover this deviation became constant while the H/D ratio is in range from 0.4 to 0.56.

A graphical representation of deviation between analytical and experimental pressure drop for spherical particles (1mm) is presented in figure 4.2 for a particular bed height 5.5 cm.

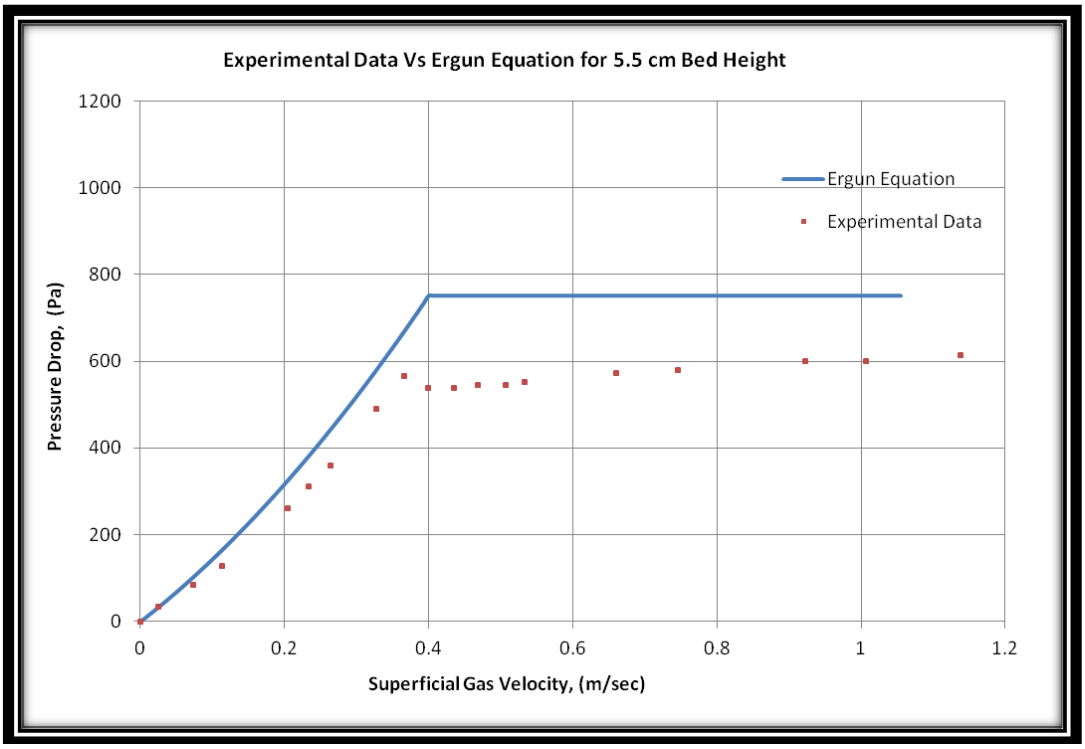

Figure 4.2: Analytical Vs. Experimental Pressure Drop for Spherical Particles.

The analytical result is derived from Ergun equation (equation 4) which is a function of particle diameter, bed diameter, densities, superficial gas velocities and void fraction. In experimental result all the parameter is taken same as analytical. But in experimental result the minimum fluidization occurs much early than analytical. This deviation comes out for void fraction changing during experiment. Changing of void fraction is observed by high speed imaging system. From the static bed situation when superficial gas velocity is zero imaging was taken with high speed camera and superficial gas velocity was increased gradually. A small increase in bed height is observed just before minimum fluidization which indicates the changing in void fraction. Because of increasing in void fraction, minimum

fluidization happens early in experiment. For analytical, void fraction remain constant. Figure 4.3 shows the increased bed height just before minimum fluidization.

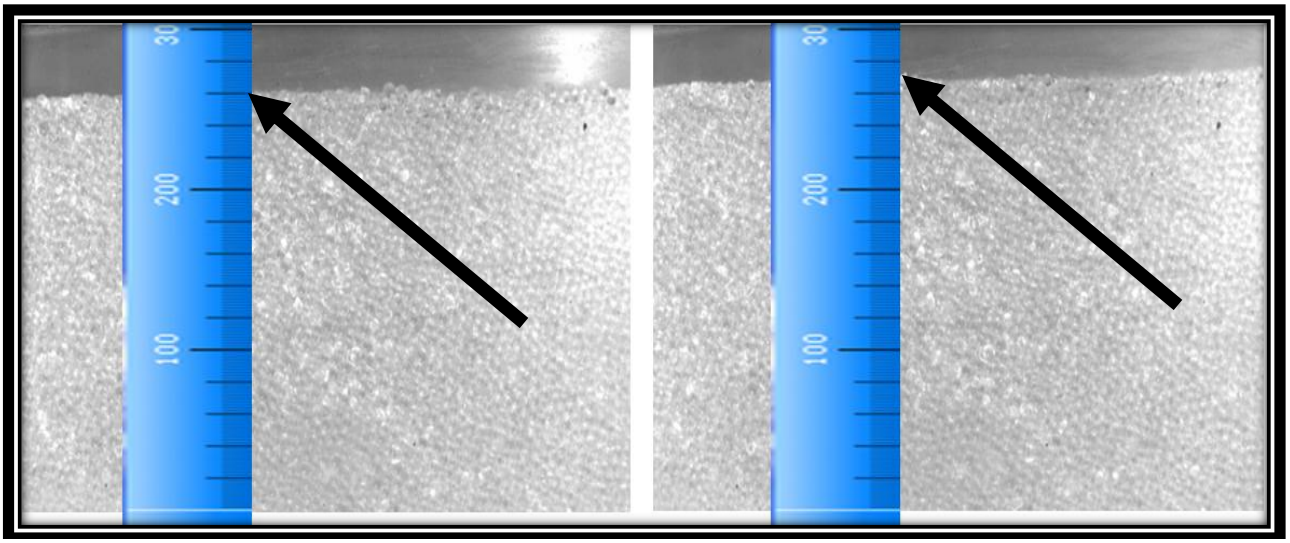

Figure 4.3: Increased Bed Height before Minimum Fluidization for Spherical Particles

As minimum fluidization velocity is an important parameter for fluidized bed, figure 4.4 is plotted to find out the effect of bed height on minimum fluidization velocity.

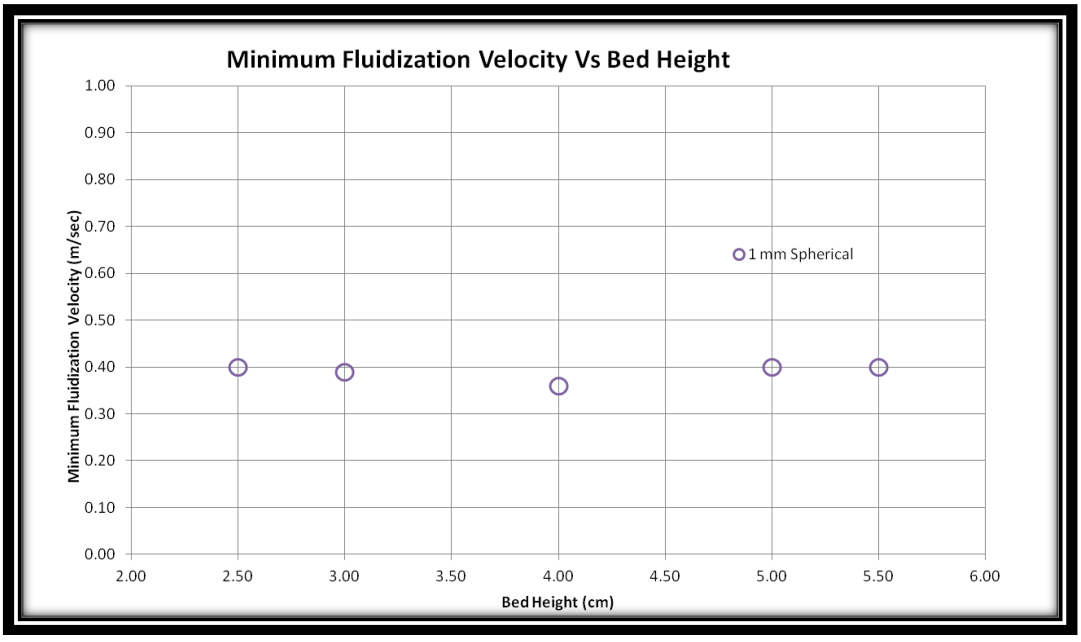

Figure 4.4: Minimum Fluidization velocity vs. Bed Height for Spherical Particles

From figure 4.4 it is shown that minimum fluidization velocity following nearly a constant line for increasing bed height and it can be concluded that minimum fluidization velocity is independent on bed height for spherical particle.

4.2 EFFECT OF BED HEIGHT FOR NON-SPHERICAL PARTICLES

The effect of bed height was also investigated for non-spherical particles. This section will describe about one range of non-spherical particles with 850-1000 µm. Experiment was done as like as spherical particle. At first particles were filled with desired height and shacked the bed column for couple of times. Pressure drop was measured with increasing superficial gas velocities. Figure 4.5 shows the experimental results of pressure drop vs. superficial gas velocities for non-spherical particles. A clear description of figure 4.5 will be found in table 4.2 for non-spherical particles with different bed height ranges from 2.5 cm to 5.5 cm bed height

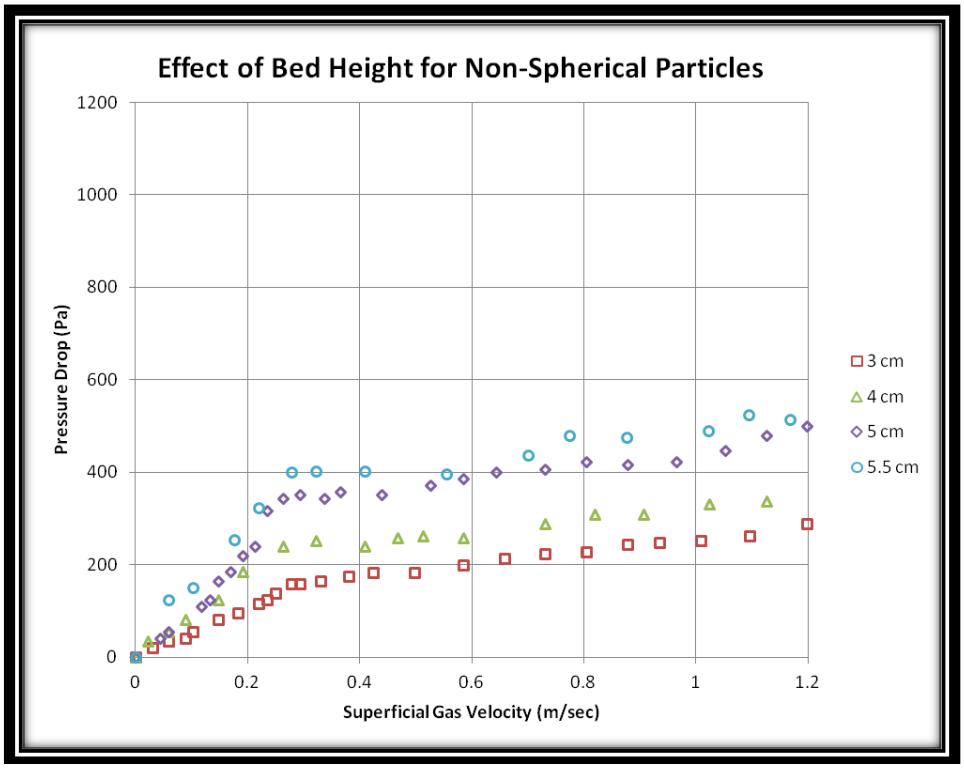

Figure 4.5: Effect of Bed Height for Non-Spherical Particles (850-1000µm)

Table 4.2: Analytical and Experimental Pressure Drop for Non-Spherical Particles (850-1000µm)

Bed Height (cm)	Analytical Min. fluidization velocity, m/sec	Exp. Min. Fluidization Velocity (m/sec)	analytical pressure drop	Exp. Pressure Drop/Pa	Deviation	Ratio of Bed Height and Bed Diameter
2.5	0.34	0.29	258	110.31	57.24%	0.20
3	0.34	0.32	309	165.5	46.44%	0.24
4	0.34	0.32	412	251	39.08%	0.32
5	0.34	0.29	516	351.6	31.86%	0.40
5.5	0.34	0.32	567	403	28.92%	0.44

From Table 4.2 it is shown that deviation between analytical and experimental decrease with increasing bed height. This indicates H/D ratio also plays an important role. A graphical representation of deviation between analytical and experimental is shown in figure 4.6 for single bed height.

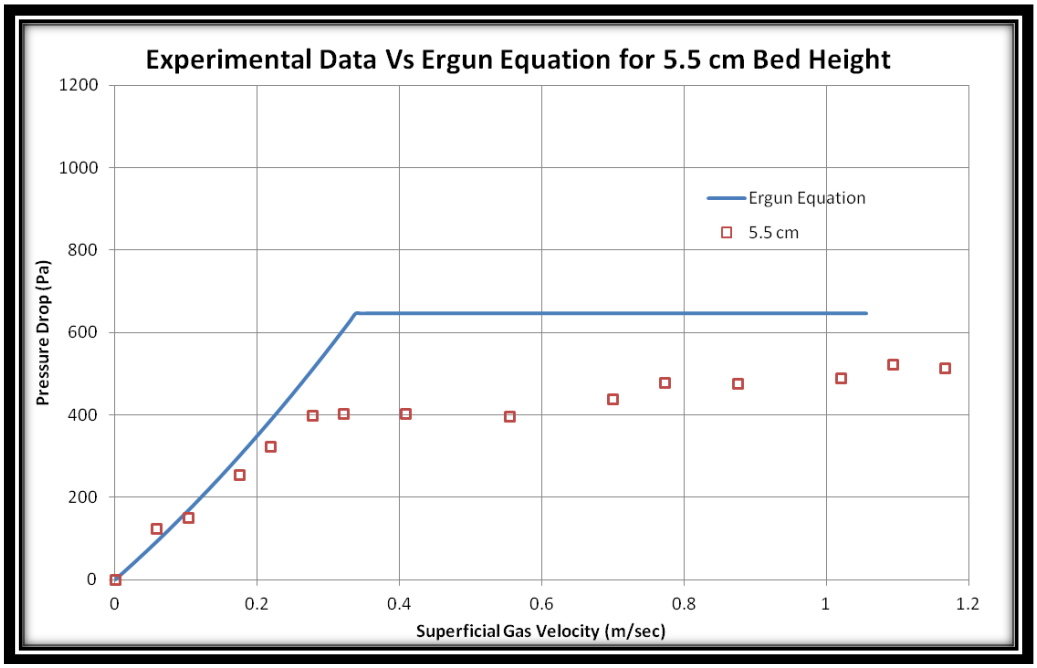

Figure 4.6: Analytical Vs. Experimental Pressure Drop for Spherical Particles.

Reason of deviation was found for spherical particles with high speed imaging. This method was also implied for non-spherical particles. Like spherical test particles there was no increased bed height observed before incipient minimum fluidization but channeling observed right before incipient minimum fluidization. Shape of spherical particles is uniform and they are densely packed in fluidized bed. Because of their uniformity and densely packing no channeling happens for spherical. On the other

hand shape of non-spherical particles is not uniform and they are not densely packed like spherical. Instead of having increased bed height before minimum fluidization a channeling happens where the particles are loosely packed. Thus make a change in void fraction and minimum fluidization happens earlier as expected.

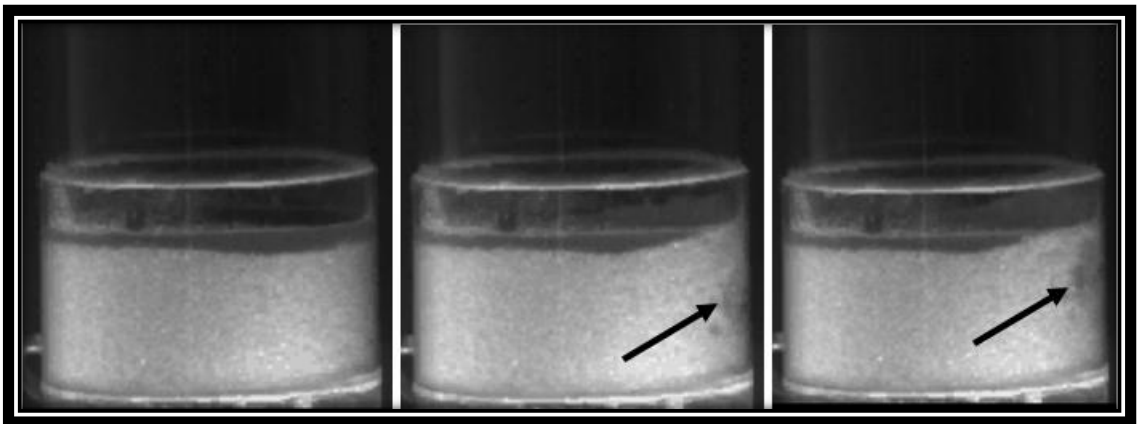

Figure 4.7: Channeling before Minimum Fluidization for Non-Spherical Particles

A graphical presentation of minimum fluidization with increasing bed height is also presented in figure 4.8 for non-spherical test particles.

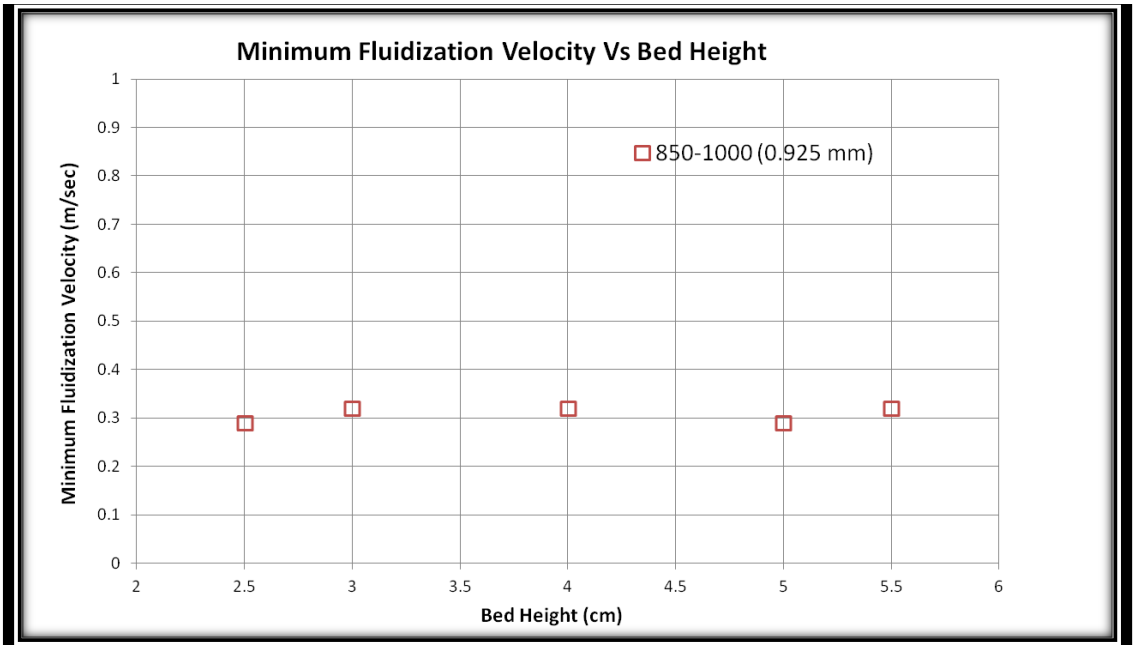

Figure 4.8: Minimum Fluidization velocity vs. Bed Height for Non-Spherical Particles

From figure 4.8 it is shown that minimum fluidization velocities remain nearly same with increasing bed height. It can be concluded that like spherical particles non-spherical particles are independent on increasing or decreasing bed heights.

4.3 EFFECT OF PARTICLE SHAPE

To investigate the effect of particle shape a specific range of non-spherical test particles were made by mixing two ranges of particles. Bidisperse test particles were made by mixing 0.85-1.0 mm and 1.0 -1.18 mm ranges particles where the mean diameter of this bidisperse particles 1.01 mm. This attempt was done to investigate the effect of spherical and non-spherical particles with same size. By making a comparison between spherical and non-spherical particles with same size we will find out the effect of particle shape where the effect of particle size is negligible. Table 4.3 shows the experimental measurement for both shapes at different bed height.

Table 4.3: Experimental Results for Spherical and Non-Spherical Particles with Same Size

		Spherical (1 mm)		Non-Spherical (≈ 1 mm)	
SL	Bed Height	Min. Fluidizatoin velocity for Spherical	Bed Pressure Drop for Spherical	Min. Fluidizatoin velocity for Non-Spherical	Bed Pressure Drop for Non-Spherical
1	2.5	0.40	193.00	0.25	151
2	3	0.39	227.00	0.26	241
3	4	0.36	365.42	0.26	344
4	5	0.40	524.00	0.29	427.47
5	5.5	0.40	537.80	0.26	544

From table 4.3 it is shown that although both test particles have the same size there is difference between minimum fluidization velocity and also in bed pressure drop for different bed height. A graphical plot also presented in figure 4.9 for a specific bed height 5 cm.

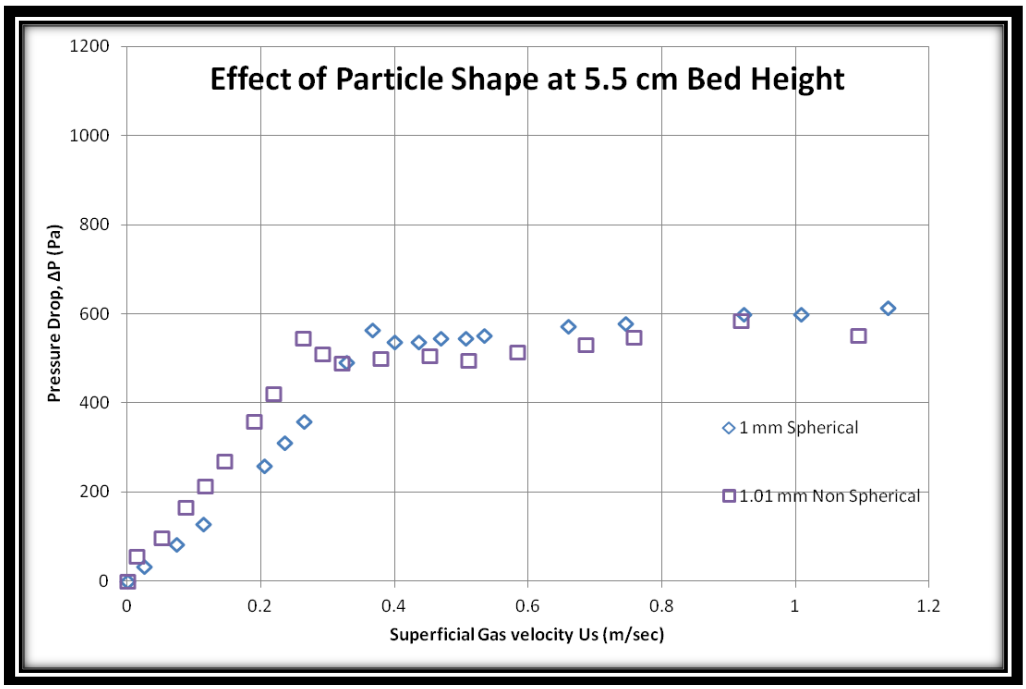

Figure 4.9: Pressure Drop vs. Gas Velocity for Spherical and Non-Spherical Particles with same size at 5.5 cm Bed Height

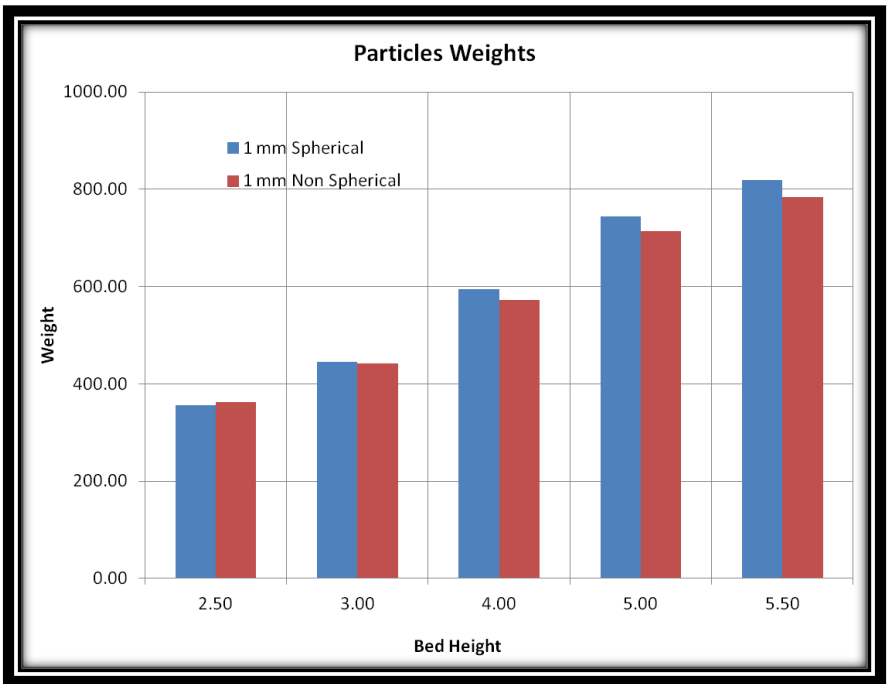

Figure 4.10: Particles Weight at Different Bed Height for Spherical and Non-Spherical Shape

Experimental measurement points of non-spherical particles follow the point with spherical particles. But minimum fluidization occurs for non-spherical much earlier than spherical particles. At all bed height from 2.5 cm to 5 cm particles weight were measured for both shape of particles. At all height they have near same weight of particles. Figure 4.10 represents the measured weight of both particles shape at different bed height. Although both test particles have same size and same weight at each bed height a deviation has observed in minimum fluidization velocities for each bed height (Table 4.3 and figure 4.9). Minimum fluidization happens earlier for non-spherical shape. This early minimum fluidization is the result of higher void fraction. Non-spherical particles are loosely packed than spherical particles. Thus non-spherical particles have higher void fraction than spherical particles and early minimum fluidization happens for this non-spherical particles.

4.4 EFFECT OF BED DIAMETER

Before laboratory scale fluidized bed (figure 3.2) a pilot scale fluidized bed were made (figure 3.4). To observe the effect of bed diameter on fluidized bed, spherical test particles with 1 mm nominal diameter was tested in both fluidized bed. The two fluidized beds contain column diameter with 12.4 cm and 3.4 cm. Figure 4.11 shows graphical plot on effect of bed diameter at 5 cm bed height.

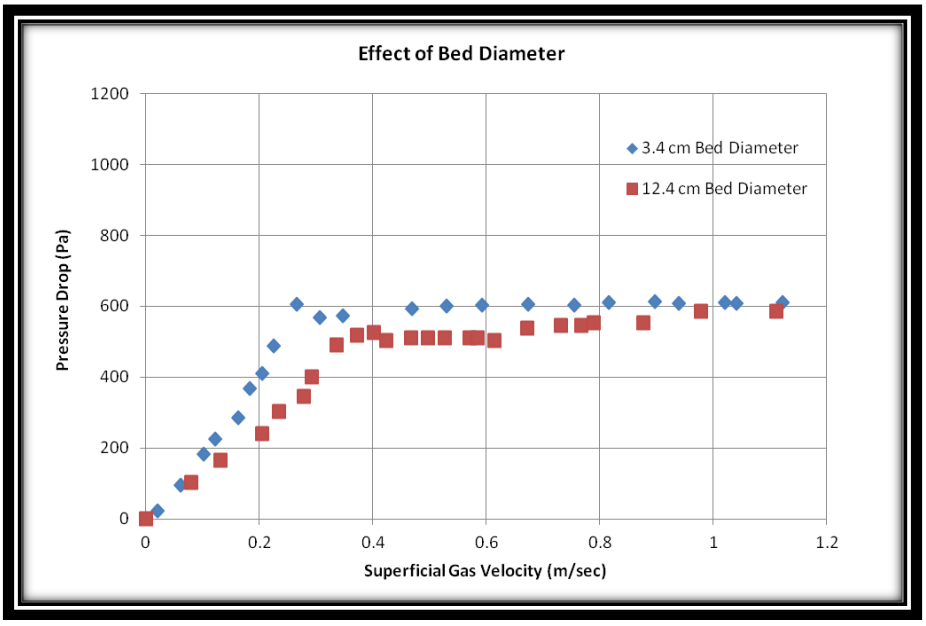

Figure 4.11: Effect of Bed Diameter at 5 cm Bed Height

From figure 4.11 it can be seen that by decreasing the bed diameter pressure drop increased and minimum fluidization velocity decreased. However, in literature it has been some different results on the effect of bed diameter. In some studies it has been found, minimum fluidization velocity increase with decreasing bed diameter. Our present experimental observation consist large particle size, variations in sphericity, larger difference in bed diameter, larger difference in bed height over bed diameter ratio. A wide range of bed diameter with different bed height observation may reveal possible empirical correlations for fluidized bed on bed diameter.

4.5 HIGH SPEED VISUALIZATION OF FLOW REGIMES

Different fluidization regimes were described in section 2.4.2. High speed imaging technology was selected to investigate the bed behavior in different fluidization regimes. Among different regimes two regimes were selected for investigation. 1) Incipient Minimum Fluidization and 2) Bubbling Fluidization. Both spherical (1 mm) and non-spherical particles (850-1000 μm) were used as test particles. These two regimes were selected because they play an important role on hydrodynamics behavior of fluidized bed.

A high-speed digital image optical technique has been used to observe 12.4 cm bed. A high speed camera (5 KHz) with couple of fluorescent light focusing on test section was used for this high speed observation. Some consecutive images of predetermined fluidization regimes for spherical and non-spherical particles were presented bellow

4.5.1 Incipient Minimum Fluidization

This regime happens at point of minimum fluidization and at that point upward fluid drag force is equal to the total weight of the particles. Figure 4.12 and 4.13 shows consecutive images from static bed to incipient fluidization state for both spherical and non-spherical particles. Images were arranged from left to right.

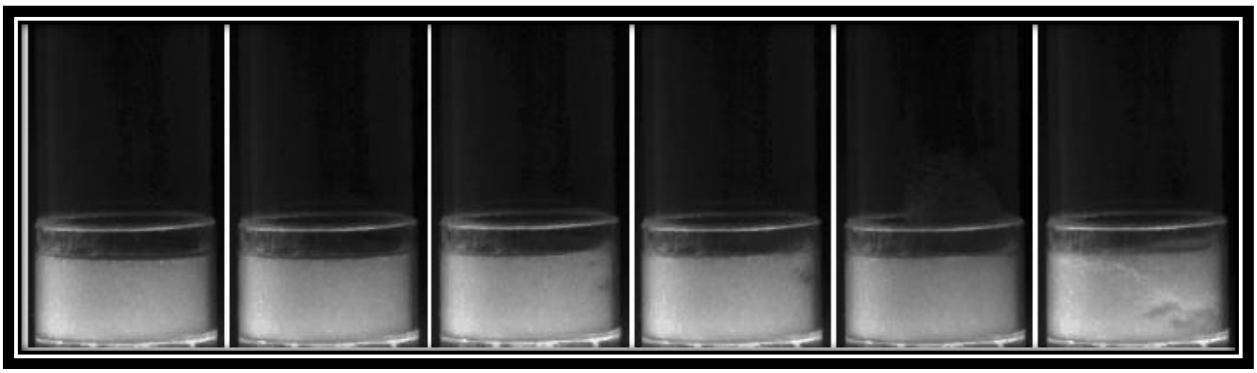

Figure 4.12: Spherical Particles (1 mm)

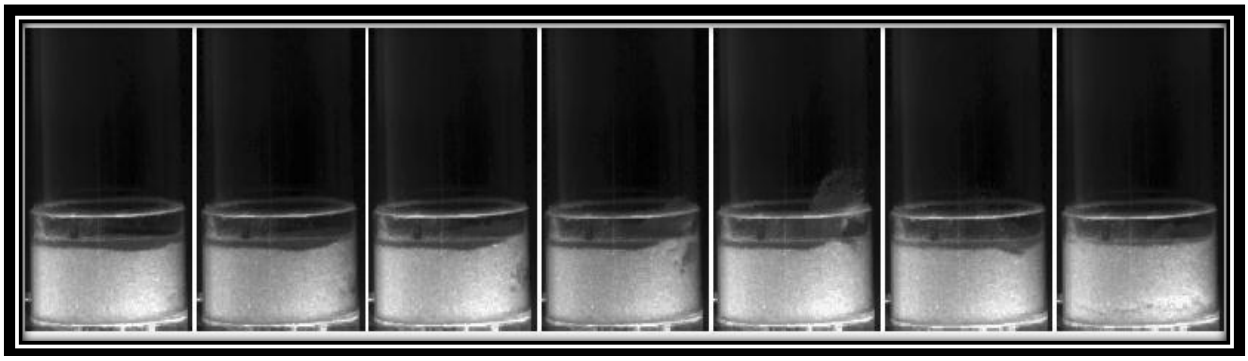

Figure 4.13: Non-Spherical Particles (850-1000 μm)

For spherical particles a significant observable increase in bed height was found as the superficial gas velocity increased. This is due to densely packed for their uniform shape compare to non-spherical particles. For non-spherical particles no observable bed height was found. Channeling observed for both spherical and non-spherical particles. Much higher channeling observed for non-spherical particles compare to spherical particles. Because of their irregular shape they are loosely packed and much higher channeling happens near with wall.

Right after channeling for both spherical and non-spherical bubbles appears at bottom part of the bed. At this point minimum fluidization appears. From the plot of pressure drop with increasing superficial gas velocity a smooth minimum fluidization found for spherical particles for their reduced channeling.

4.5.2 Bubbling Fluidization

Bubbling fluidization happens with higher gas flow rate beyond minimum fluidization. Figure 4.14 and 4.15 shows consecutive images from minimum fluidization to bubbling fluidization for both spherical and non-spherical particles. It is observed that bubble appears at bottom and it rise from bottom to top of the bed. It is also observed that bubbles coalescence in vertical and horizontal directions. When bubbles rises up, particles weight in upper part get reduces which helps bubbles to get bigger in size by merging tailing bubbles with leading bubbles. For horizontal coalescence the bubbles merge with the adjacent bubbles.

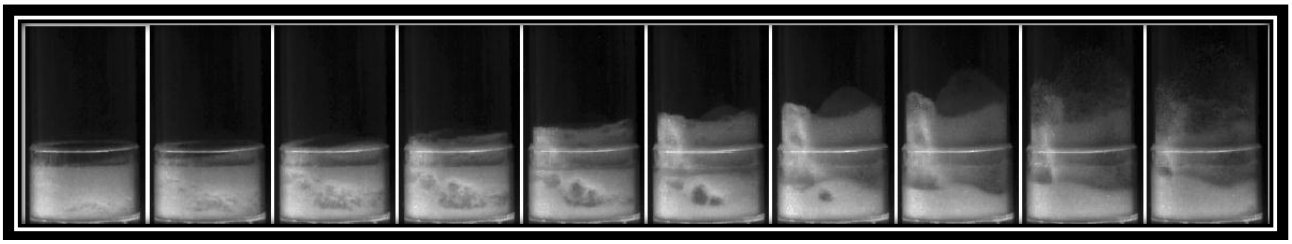

Figure 4.14: Spherical Particles

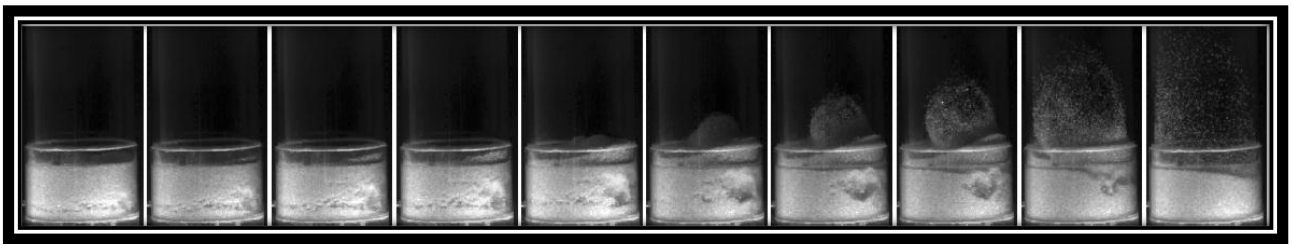

Figure 4.15: Non-Spherical Particles

4.6 FLOW FIELD VISUALIZATIN WITH SHADOWGRAPHY

For qualitative visualization and quantitative measurement of flow field in fluidized bed a non-intrusive technique was used. Shadowgraphy with backlight imaging method was used for observation. Section 3.4 describes about shadow sizing technology. This technology capture shadow images of test section separated with time and finally those consecutive images are processed with commercial software DynamicStudio. This shadow sizing technology is suitable for low particle density region. Shadowgraphy was done for both spherical and non-spherical particles.

4.6.1 Shadow Sizing of Spherical Particles

1 mm spherical particles were used as test particles with 5.5 cm bed height. Two test sections were selected for this observation. One section was 21 cm above from top surface of test particles and the other one is just after top surface of test particles. Position 21 cm above from top surface of test particles was chosen to get dilute section with full fluidization. At full fluidization with higher gas velocity particles were trapped on the top mesh catch. At that regime images were taken to visualize the flow field and also to get quantitative measurements of particles flow. Figure 4.16 shows successive images were taken with triggering rate 1000 Hz.

Figure 4.16: Shadow Images for Spherical Particles in Dilute Section

From thousands of images only three consecutive images were shown in figure 4.16. From these shadow images particles size, their instantaneous velocities were measured with shadow processing in DynamicStudio commercial software. Figure 4.17 shows the shadow processed results of 1st image in figure 4.16

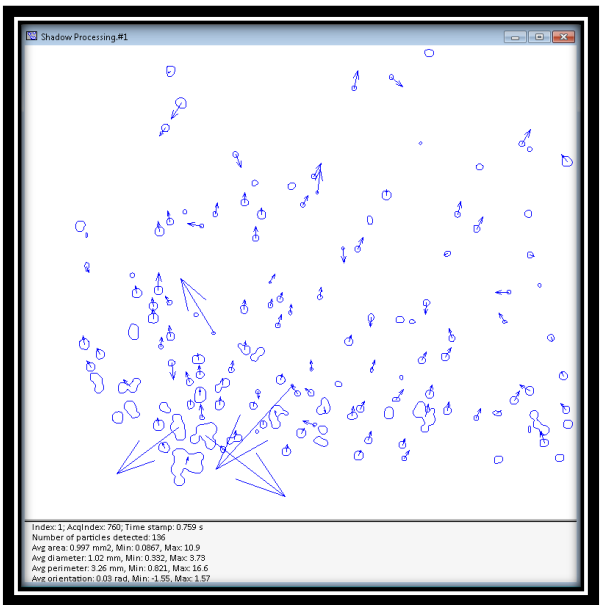

Figure 4.17: Shadow Processed Results for Instantaneous Moment

Figure 4.17 indicates particles contour with their mean diameter and velocity direction. 1 mm spherical particles were used as test particles and shadow processed result (figure 4.17) from a double frame image shows the mean diameter 1.02 mm which indicates shadow sizing can detect particles exact size. A diameter statistics is also presented in figure 4.18 from 64 shadow images.

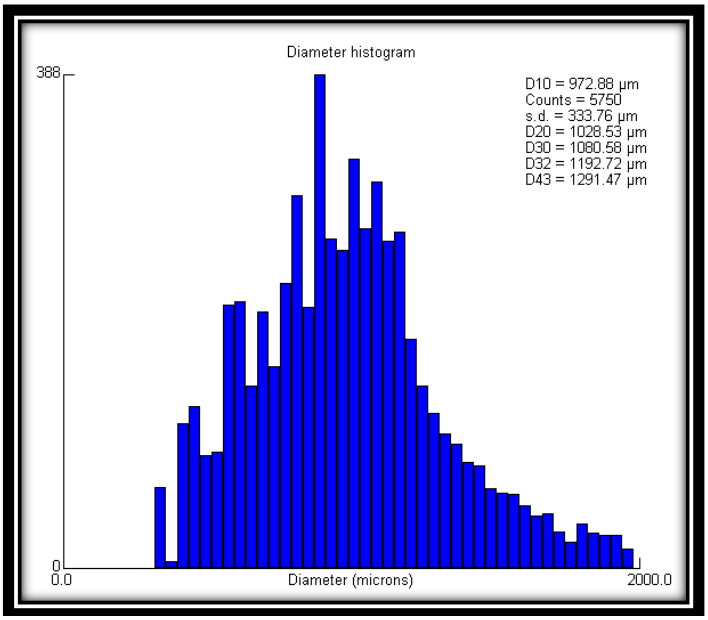

Figure 4.18: Diameter Statistics for Spherical Particles.

From figure 4.18 it has been found the mean diameter 972.88 µm with standard deviation 333 µm. While the images were taken the camera was focused in one plane. In image where the particles are out of focus they became blurred and show the diameter larger or smaller than the actual. But the amount of these blurred particles in results is less because when the intensity is less from blurred particles it will not count.

Particles are moving in horizontal and vertical directions. From numerical result of each shadow processed image it is possible to find out instantaneous average horizontal and vertical velocity magnitude. The average horizontal and vertical velocities of particles shown in figure 4.17 are 0.33 m/sec and 0.37 m/sec respectively.

Figure 4.19 also shows the size-velocity correlation from 62 shadow processed images.

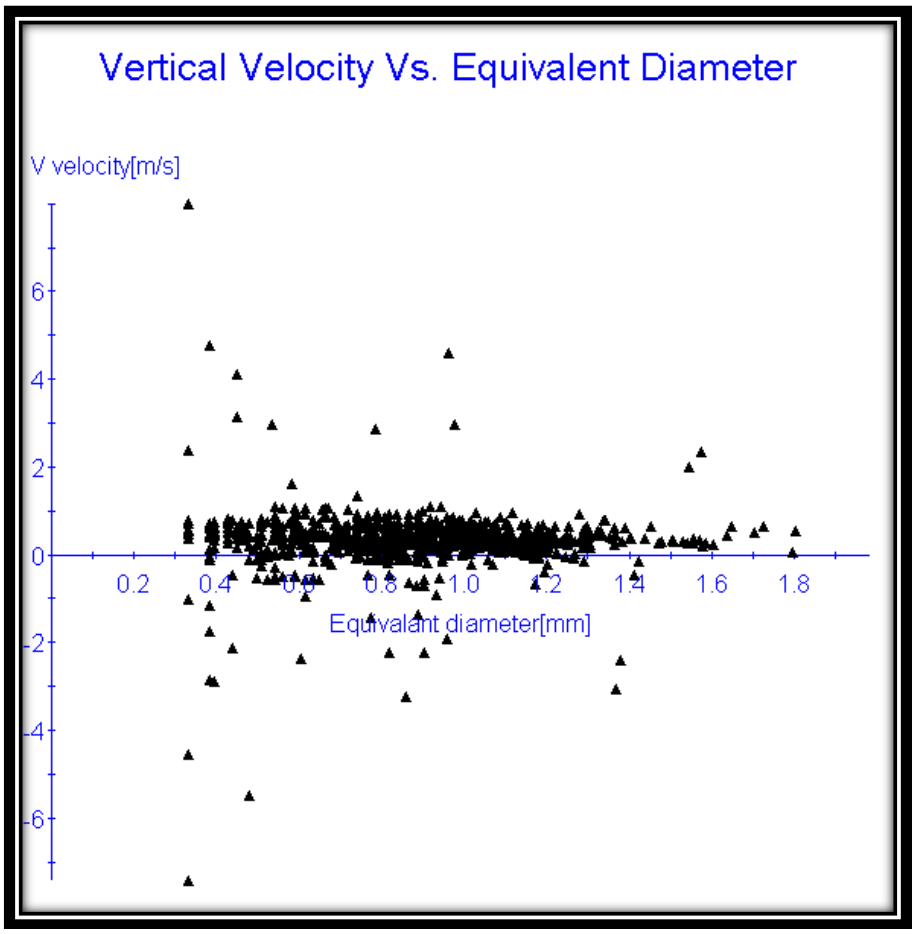

Figure 4.19: Vertical Velocities over Equivalent Diameter for Spherical

Figure 4.19 shows the particles velocity in vertical direction. Most of particles velocity region near 0.5 m/sec. Negative velocity indicates that particles are in downward direction. Figure 4.20 also shows the horizontal velocity correlation with size from 64 images.

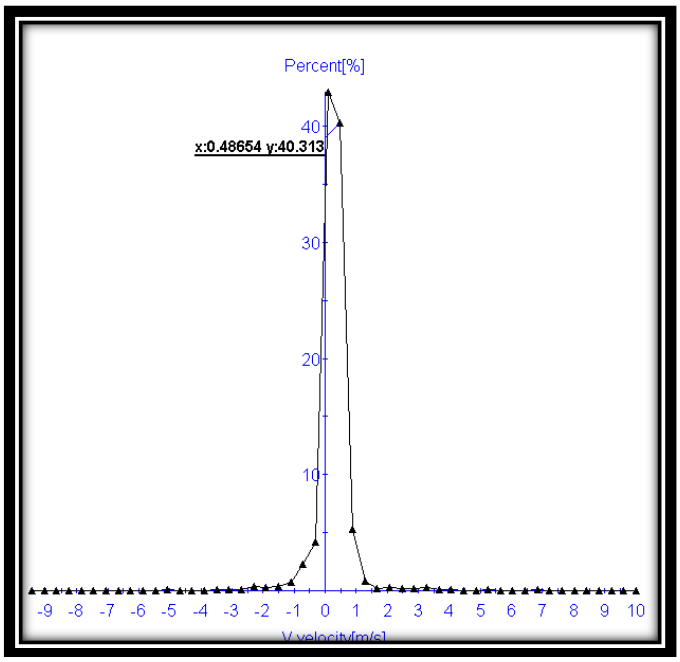

Figure 4.20: Vertical Velocity over Percentage.

Figure 4.20 shows the particles velocities over percentage where it has been found over 42 percent particles have velocity 0.089 m/sec and over 40 percent particles have velocity 0.48 m/sec in vertical direction.

Horizontal velocities over particle size are also in ranges from 0.2 to 0.3 m/sec and the negative sign indicates the direction. Figure 4.21 shows the horizontal velocities over equivalent diameter. Figure 4.22 also shows the particle velocity over percentage. It has been found from figure 4.22 that over 61 percent particles have velocity 0.047 m/sec in horizontal direction.

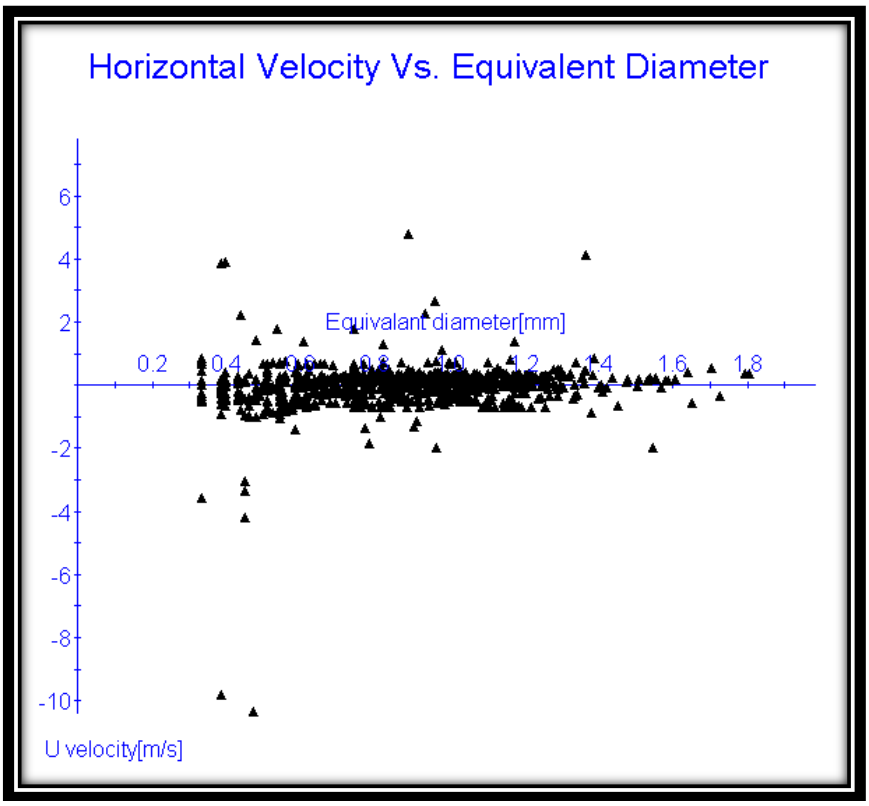

Figure 4.21: Horizontal Velocities over Equivalent Diameter for Spherical Particles

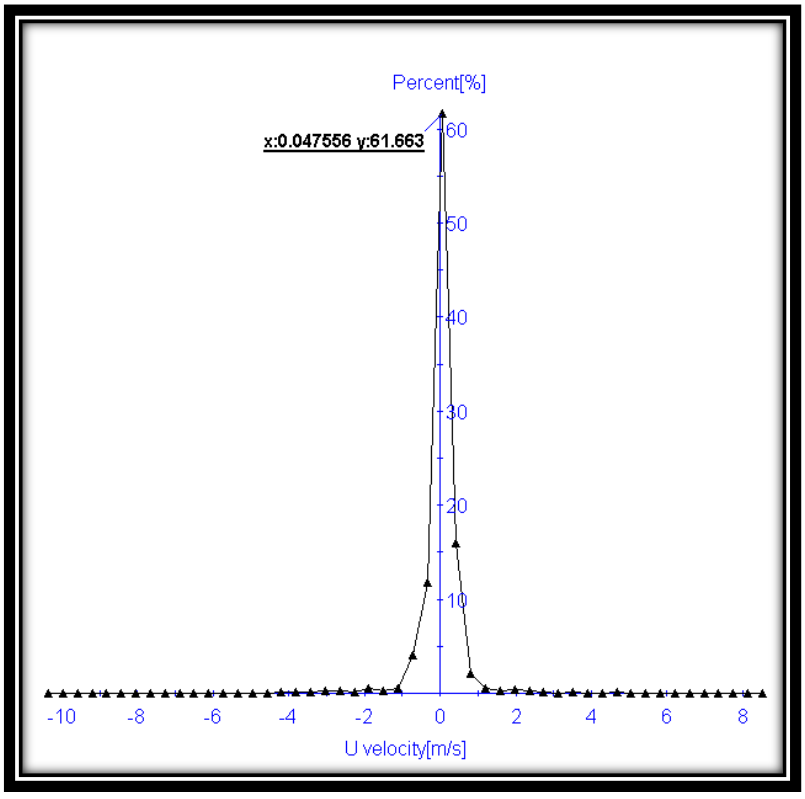

Figure 4.22: Horizontal Velocities over Percentage

4.6.2 Shadow Sizing of Non-Spherical Particles

850-1180 μm non-spherical particles with 1.01 mm nominal diameter were used as test particles. Calibration images were taken with same camera position, same focusing plane as used in spherical particles. Qualitative and quantitative measurements for non-spherical particles are presented in following figures.

Figure 4.23: Shadow Images of Non-Spherical Particles in Dilute Section

These shadow images were taken with 1000 Hz trigger rate same as used in spherical particles. Figure 4.23 shows three consecutive images with .002 sec interval. One single shadow processed image is also shown in figure 4.24 with their average mean diameter, particles contour and their velocity directions.

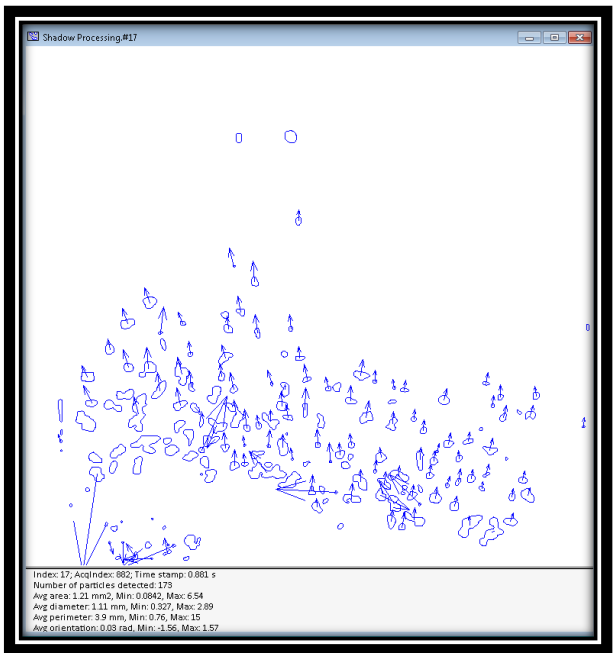

Figure 4.24: Shadow Processed Results for Instantaneous Moment

Figure 4.24 shows the shadow processed result of 3rd image in figure 4.21 with average mean diameter 1.11 mm. In this observation 850 -1180 µm non-spherical particles were used where the mean sieve diameter was 1.01 mm. A diameter statistics is also presented in figure 4.25.

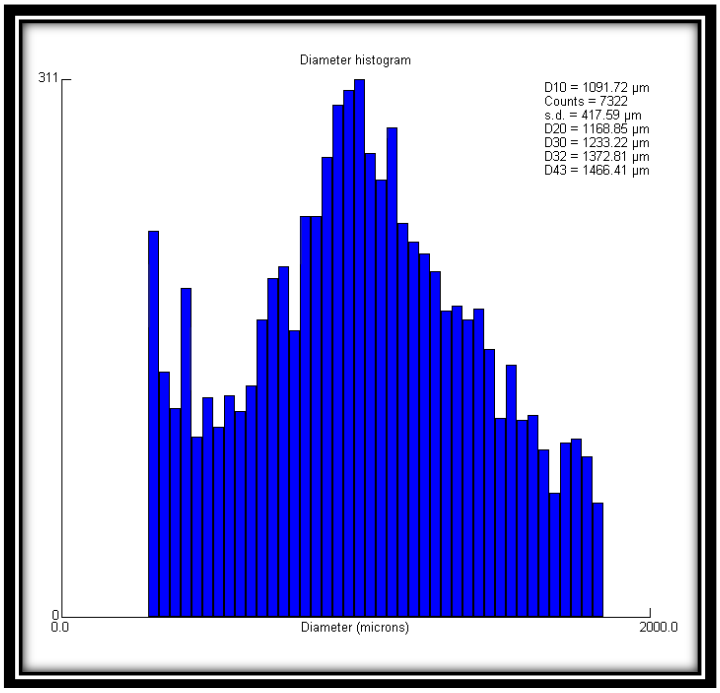

Figure 4.25: Diameter Histogram for Non-Spherical Particles

Figure 4.25 shows the diameter histogram for non-spherical particles resulting from 65 shadow processed images with particles counting, mean diameter 1091.72 µm and standard deviation 417.59 µm.

Size-velocity correlation also found from shadow sizing. Figure 4.26 shows the vertical velocities over particles size.

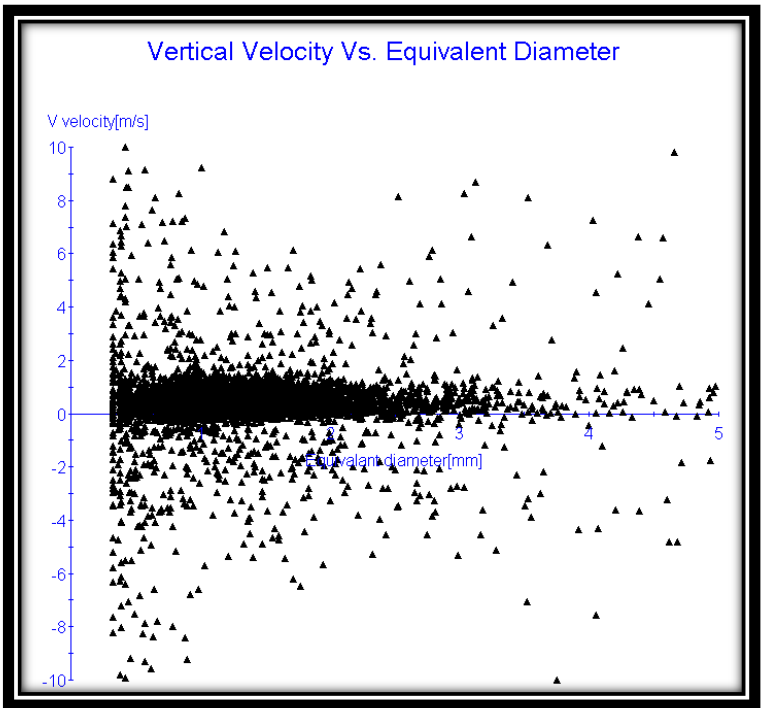

Figure 4.26: Vertical Velocities over Equivalent Diameter for Spherical

Most of the particles velocities ranges below 1 m/sec and negative velocities indicates downward direction of particles. Again more clear view will be found in figure 4.27 with velocities over percentage plot.

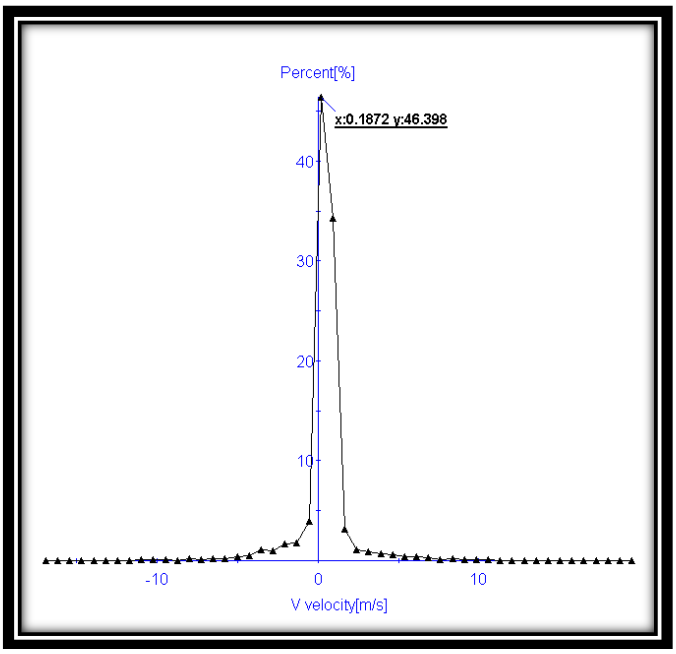

Figure 4.27: Vertical Velocities over Percentage.

From figure 4.27 it has found that over 46 percent particles have velocity 0.1872 m/sec in vertical direction. Figure 4.28 shows horizontal velocities over equivalent diameter and figure 4.29 shows velocities over percentage.

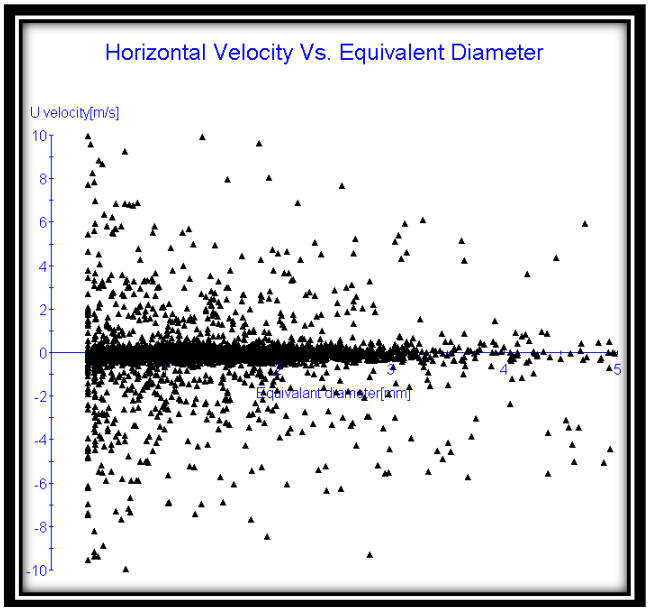

Figure 4.28: Horizontal Velocities over Equivalent Diameter for Non-Spherical Particles

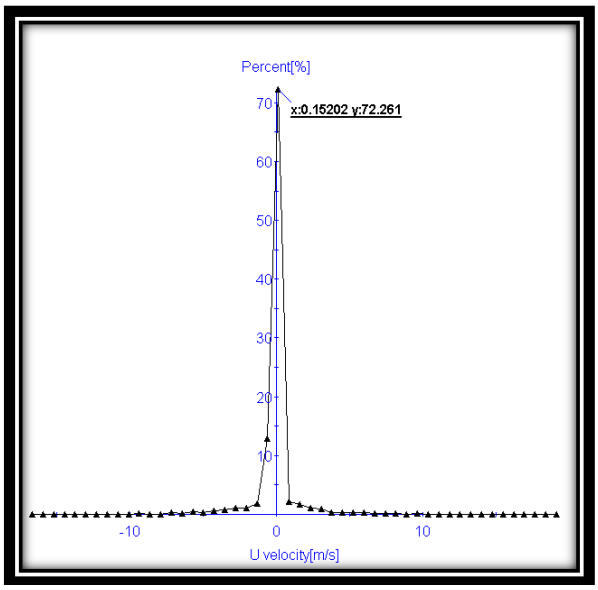

Figure 4.29: Horizontal Velocities over Percentage for Non-Spherical

From figure 4.29 it has been found over 72 percent particles have velocity 0.15 m/sec in horizontal direction.

4.6.3 Bubble Collapsing in Bubbling Fluidization

After minimum fluidization with increased superficial gas velocities bubble appears at the bottom of bed, rises up and collapse for both spherical and non-spherical particles. Figure 4.30 and 4.31 shows the bubbles collapse for both spherical and non-spherical particles.

Figure 4.30: Bubble Collapsing for Spherical Particles

A bubble collapsing for spherical particles looks uniform. Before collapsing they form a half circle shape. Particles don't scattered and they fall in a stream line. This happens because spherical

particles are uniform in shape and they densely packed which prevent them to scatter while bubble collapse.

Figure 4.31: Bubble Collapsing for Non-Spherical Particles.

On the other hand when bubbles collapse in non-spherical particles they scattered randomly. Although at a moment bubbles seems like a half circle but latter the shape disappear and particles scattered. This is happen due to loosely packed. As non-spherical particles are irregular in shape they loosely packed in bed with much higher void fraction then spherical. Shadow processing of bubbles collapsing images is very hard as particles density is higher near bubbles. For shadow processing less density particles zone is required.

Chapter 5: Conclusion & Future Work

5.1 CONCLUSION

To observe hydrodynamics behavior of gas-solid fluidized bed an investigation was done on laboratory scale fluidized bed with different particle sizes and shapes. The laboratory scale fluidized bed was designed and constructed in university machine shop. To investigate bed behavior pressure drop across the bed was measured with increasing superficial gas velocity. Pressure drops were measured for different bed height, different particle size and for different particle shapes. Insertion type flow meter and digital differential manometer were used with data logger to measure flow rate and pressure drop respectively.

1 mm spherical particles with different bed height from 2 cm to 7 cm tested in fluidized bed. Pressure drop increases with increasing superficial gas velocity until the particles are fixed into bed. Pressured drop suddenly falls from its peak point became constant with further increasing gas velocity. At the peak point the pressure drop is equal the total weight of the particles. After this point with increasing gas velocity particles bonding collapse and pressure drop suddenly falls and began constant. Same thing happens for each bed height. While all the measurement of each bed height plot together than it is shown that bed pressure drop increase with increase bed height. This is because highest pressure drop is equal to the weight of the particles. With increasing bed height particles weight increase and bed pressure drop increase. On the other hand, from the plot it is clearly visible that minimum fluidization velocities remain constant with increasing bed height which indicates that minimum fluidization velocity is independent of bed height.

Non-spherical particles were also used with different sizes range. Same measurements were taken with different bed height for all ranges. From pressure drop vs. superficial gas velocity plot the result has found same as spherical. Pressure drop increase with increasing bed height and minimum fluidization velocity is independent on bed height. Minimum fluidization velocities remain constant with

increasing bed heights. For changing particle size minimum fluidization velocity and pressure drop decreases with decreasing particle size.

Experimental results were compared with theoretical results and the difference between theoretical and experimental was found. High speed imaging was used to clarify the reason of this difference for both spherical and non-spherical particles. Bed expansion and channeling right before minimum fluidization is responsible for this difference.

1 mm spherical particle result of one bed height from laboratory scale fluidized bed was compared with another pilot scale fluidized bed with different bed diameter. This comparison gives the effect of bed diameter. It has been found that minimum fluidization velocity decrease with decreasing bed diameter. Although in literature it has been found that minimum fluidization increase with decreasing bed diameter. Our bed geometry, particle parameters are different compare to literature and large size of particles were used. A wide ranges of particle size, bed diameter need to investigate to make a correlation of minimum fluidization over bed diameter.

A non-intrusive technology shadow sizing was used to visualize flow field for both spherical and non-spherical particles. With higher gas velocity when particles are trapped into top mesh of bed column shadow images were taken in that regimes in dilute section. Flow field of instantaneous moment were found spherical and non-spherical particles. The working principle of shadow sizing can measure any size of particles. Qualitative and quantitative results were found with vertical and horizontal particles velocity. Shadow sizing technology was also used to observe bubble collapse. A difference has found during collapsing of bubbles between spherical and non-spherical particles and this is due to densely and loosely packed of particles.

5.2 FUTRUE WORK

For current experiment only one single particle density was considered but in future particles with different density can be used to observe the effect of particle density over different height and different bed diameter.

Cylindrical bed was used in current experiment. In future different bed geometry like rectangular bed and cylindrical bed with conical shape bottom can be used to investigate bed hydrodynamics.

Different ranges of particles with different sphericity ranges were categorize and stored in glass bottles. Shadow sizing technology will be used to measure the terminal velocity of free falling non-spherical particles of each particle ranges and each sphericity ranges. From terminal velocity of different ranges a drag model will be proposed for free falling non-spherical particles.

Finally the entire experimental data and drag model will be incorporated with MFIX (Multiphase Flow with Interphase eXchanges)

Bibliography

1. **Oka, Simon N.** *Fluidized Bed Combustion.* s.l. : Marcel Dekker, Inc, 2004. p. 1. ISBN: 0-8247-4699-6.
2. U.S. Department of Energy. *Gasification Technology R&D.* [Online] http://www.fossil.energy.gov/programs/powersystems/gasification/index.html.
3. *Discrete Particle Simulation of Solids Motion in a Gas-Solid Fluidized Bed.* **L. Sunmum, C. Ativuth, U. Kosol, T. Yutaka, K. Toshihiro, T. Wiwut.** 6, s.l. : Chemical Engineering Science, 2003, Vol. 58, pp. 915-921.
4. Clean-Energy.US websit. *Clean Energy. US website http://www.clean-energy.us/facts/gasification.htm.* [Online] http://www.clean-energy.us/facts/gasification.htm.
5. Gasification Technologies Council. *http://www.clean-energy.us/index.htm.* [Online] http://www.gasification.org/page_1.asp?a=24&b=1&c=85.
6. "ZEEP". *Zero Emission Energy Plants.* [Online] http://www.zeep.com/zeep-technology/gasification-vs-combustion.php.
7. "Gasification". *Wikipedia, the free encyclopedia.* [Online] http://en.wikipedia.org/wiki/Gasification.
8. The National Energy Technology Laboratory (NETL). *The Energy Lab.* [Online] http://www.netl.doe.gov/technologies/coalpower/gasification/gasifipedia/4-gasifiers/index.html.
9. The National Energy Technology Laboratory (NETL) website. [Online] http://www.netl.doe.gov/technologies/coalpower/gasification/gasifipedia/4-gasifiers/4-1-1_fmb.html.
10. The National Energy Technology Laboratory (NETL) website. [Online] http://www.netl.doe.gov/technologies/coalpower/gasification/gasifipedia/4-gasifiers/4-1-2_entrainedflow.html.
11. The National Energy Technology Laboratory (NETL) website . [Online] http://www.netl.doe.gov/technologies/coalpower/gasification/gasifipedia/4-gasifiers/4-1-3_fluidizedbed.html.
12. **Crowe, Clayton T.** *Multiphase Flow Handbook.* Boca Raton, Florida : Taylor & Francis Group, 2006. 10:0-8493-1280-9.
13. **yang, Wen-Ching.** *Handbook of Fluidization and Fluid-Particle Systems.* New York : Marcel Dekker, Inc, 2003. ISBN: 0-8247-0259-X.
14. Outotec. *Outotec and More out of Ore.* [Online] 2007. http://www.outotec.com/36280.epibrw.
15. **Gidaspow, Dimitri.** *Multiphase Flow and Fluidization, Continuum and Kinetic Theory Descriptions.* 1994. ISBN 0-12-282470-9.
16. **Hetsroni, Gad.** *Handbook of Multiphase Systems.* s.l. : Hemisphere Publishing Corporation, 1982. ISBN 0-07-028460-1.
17. **Warren L. McCabe, Julian C. Smith, Peter Harriott.** *Unit Operations of Chemical Engineering.* New York : The Mcgraw-Hill Companies, Inc., 2005. ISBN 0-07-284823-5.
18. Ergun Equation. *Wikipedia, The Free Encycloedia.* [Online] April 2012. http://en.wikipedia.org/wiki/Ergun_equation.
19. *Experimental Study on the Effectice Particle Diameter of a Packed Bed with Non-Spherical Particles.* **Liangxing Li, Weimin Ma.** s.l. : Transp Porous Med(2011), 2011. DOI 10.1007/s11242-011-9757-2.
20. *The Expansion of Gas-Fluidized Beds in Bubbling Fluidization.* **D.J. Gunn, N. Hillal.** 16, s.l. : Chemical Engineering Science, 1997, Vol. 52, pp. 2811-2822.
21. *The Gas Fluidization of Large particles.* **D. Geldart, R. R. Cranfield.** s.l. : Chemical Engineering Journal, 1972, Vol. 3, pp. 211-231.
22. *Effect of Bed Diameter, Distributor and Inserts on Minimum Fluidization Velocity.* **N. Hilal, R.R. Ghannam, M.Z. Anaabtawi.** 2, s.l. : Chemical Engineering Technology, 2001, Vol. 24, pp. 161-165.

23. *Minimum Fluidization Velocities for Gas-Solid 2D Beds.* **G. Ramos, G. Ruiz, J.P. marques, G. Soler.** s.l. : Chemical Engineering and Processing, 2002, Vol. 41, pp. 760-764.
24. *Hydrodynamic Characteristics of Spout-Fluid Bed: Pressrue Drop and Minimum Spouting/Spout-Fluidization Velocity.* **W. Zhong, X. Chen, Z. Mingyao.** s.l. : Chemical Engineering Journal, 2006, Vol. 118, pp. 37-46.
25. *Minimum Fluidization velocities and Maximum Bed Pressure Drops for Gas-Solid Tapered Fluidized Beds.* **D.C. Sau, S. Mohanty, K.C. Biswal.** s.l. : Chemical Engineering Journal, 2007, Vol. 132, pp. 151-157.
26. *Fluidization of Biomass particles in a Gas-Solid Fluidized Bed.* **W. Zhon, B. Jin, Y. Zhang, X Wang and R Xiao.** s.l. : Energy and Fuels, 2008, Vol. 22, pp. 4170-4176.
27. *The effect of Column Diametr and Bed Height on Minimum Fluidization Velocity.* **A Rao, J. S. Curtis.** 9, s.l. : AIChE Journal, 2010, Vol. 56, pp. 2304-2311.
28. *Bed Height and Material Density Effects on Minimum Fluidizaiton Velocity in a Cylindrical Fluidized Bed.* **D. Escudero, J. Heindel.** Tampa, Florida : 7th International COnference on Muliphase Flow, 2010. Paper No. 1674.
29. *Particle Size Distribution Analysis of Coarse Aggregate Using Digital Image Processing.* **C.F. Mora, A.K.H. Kwan, H.C. Chan.** 6, s.l. : Elsevier Science Ltd, 1998, Cement and Concrete Research, Vol. 28, pp. 921-932.
30. *Measurement and Geological Significance of Shape and Roundness of Sedimentary particles.* **Krumbein, W.C.** s.l. : Journal of Sedimentary Petrology, 1941, Vol. 11, pp. 64-72.
31. *Volume, Shape and Roundness of Rock Particles.* **Wadell, Hakon.** 5, Chicago : The Jornal of Geology, 1932, Vol. 40, pp. 443-451.
32. *Modellig the internal Flow Structure of Circulating Fluidized Beds.* **Franco Berruti, Nicolas Kalogerakis.** 6, s.l. : The Canadian Journal of Chemical Engineering, 1989, Vol. 67, pp. 1010-1014.
33. Dantec Dynamics. [Online] 2012. http://www.dantecdynamics.com/Default.aspx?ID=1779.
34. **Anthony J. Wheeler, Ahmad R. Ganji.** *Introduction to Engineering Experimentation.* Third Edition. s.l. : Prentice Hall, 2010. ISBN 978-0-13-174276-5.
35. Standard Deviation. *Wikipedia, the free encyclopedia.* [Online] http://en.wikipedia.org/wiki/Standard_deviation.
36. t-distribution table. *Statistics How To.* [Online] http://www.statisticshowto.com/tables/t-distribution-table/.

Appendix A

Nomenclature

R_e	Reynolds Number
U_{mb}	Bubbling Fluidization Velocity
U_{mf}/V_{mf}	Minimum Fluidization Velocity
U_{ms}	Slugging Velocity
U_k	Velocity at Transition to Turbulent Regimes
U_{tr}	Vertical Transport Velocity
f_p	Frictional Factor
ΔP	Bed Pressure Drop
ρ_f	Density of Air
ρ_p	Density of Particle
μ	Viscosity of Air
g	Gravitational Force
ϵ	Void Fraction
φ	Particle Sphericity
V_s	Superficial Gas Velocity
D_P	Particle Diameter
D_{eq}	Equivalent Diameter
L	Bed Height

Appendix B

Key Parts and Instrument Specification

Grainger 7AV38 High Pressure Blower

Description	Specification
Motor HP	5
Phase	3
Hz	60
Voltage	208-230/460
Full Load Amps	12.9-11.7/.8

Grainger 1JBF9 MILWAUKEE Butterfly Valve

Description	Specification
Valve Diameter	5 in
Flange Thickness	2.25 in
Rated PSI	200
Temperature Range	-25 to 250 F

Omega FMA 1845 Digital Mass Flow meter

Description	Specification
Units	SLM
Range	0-4000 L/min
Type	Linear
Output	0 to 5 Vdc
Maximum Pressure	500 PSIG
Operating Voltage	12 Vdc
Accuracy	±1.5% of full scale

Digital Differential Manometer

Description	Specification
Accuracy	±0.3% FS
Pressure Media	Clean, Dry, Non corrosive gas
Response Time	0.5 sec

Curriculum Vita

Md Rashedul Hasan Sarker was born in 1st January, 1985 in Dhaka, Bangladesh. He is the son of Md Habib Ullah Sarker and Meher Nigar. In 2001 he has completed his college degree from Govt. Science College, Dhaka, Bangladesh and joined Khulna University of Engineering & Technology (KUET) in 2003 to complete his Bachelor of Science Degree in Mechanical Engineering. He worked with computer controlled direct gasoline fuel injection system as his undergraduate thesis and also successfully done job responsibility in Power Generation Company in Bangladesh. To pursue higher degree he took admission in The University of Texas at El Paso (UTEP) in Masters of Science in Mechanical Engineering from spring 2011. He worked as Graduate Research Assistant at NASA Center for Space Exploration Technology Research lab for last one and half year where he focused on Investigation on a Gas-Solid Fluidized Bed Hydrodynamics Using a Non-Intrusive Technology to Visualize Flow Field. Within this period he submitted a full conference paper and presented in 50th AIAA Aerospace Sciences Meeting including the New Horizons Forum and Aerospace Exposition, January 9-12, 2012. Also he is a second author of another paper at same conference he presented. He also submitted one article for 2nd Southwest Energy Science and Engineering Symposium, 2012.

Permanent Address: 29/1-B, Malibag Chowdhurypara
DIT Road, Dhaka-1219

This thesis was typed by Md Rashedul Hasan Sarker.